

# AIX-MARSEILLE UNIVERSITY

DOCTORAL SCHOOL: Physics and Material Science

PARTENAIRES DE RECHERCHE

Laboratoire MADIREL

Submitted with the view of obtaining the degree of doctor

Discipline: Material Science

Specialty: Characterisation of porous materials

Paul A. Iacomi

Titre de la thèse: sous-titre de la thèse

Defended on JJ/MM/AAAA in front of the following jury:

Prénom NOM	Affiliation	Rapporteur
Prénom NOM	Affiliation	Rapporteur
Prénom NOM	Affiliation	Examinateur
Prénom NOM	Affiliation	Examinateur
Prénom NOM	Affiliation	Examinateur
Prénom NOM	Affiliation	Directeur de thèse

National thesis number: 2017AIXM0001/001ED62



This work falls under the conditions of the Creative Commons Attribution License -  
No commercial use - No modification 4.0 International.

# Abstract

Abstract is here.

# Acknowledgements

Acknowledgements go here

# Contents

<b>Abstract</b>	iii
<b>Acknowledgements</b>	iv
<b>1. Building a framework for adsorption data processing</b>	1
1.1. Introduction . . . . .	1
1.2. Physical models of adsorption . . . . .	2
1.2.1. The Henry model . . . . .	3
1.2.2. Langmuir and multi-site Langmuir model . . . . .	3
1.2.3. BET model . . . . .	5
1.2.4. Toth model . . . . .	7
1.2.5. Temkin model . . . . .	7
1.2.6. Jensen-Seaton model . . . . .	8
1.2.7. Quadratic model . . . . .	8
1.2.8. Virial model . . . . .	9
1.2.9. Vacancy solution theory models . . . . .	9
1.3. Characterisation of materials through adsorption . . . . .	10
1.3.1. Specific surface area and pore volume calculation . . . . .	10
1.3.2. Assessing porosity . . . . .	14
1.3.3. Predicting multicomponent adsorption . . . . .	19
1.4. pyGAPS overview . . . . .	21
1.4.1. Core structure . . . . .	21
1.4.2. Creation of an Isotherm . . . . .	23
1.4.3. Units . . . . .	25
1.4.4. Workflow . . . . .	25
1.4.5. Characterisation using pyGAPS . . . . .	26
1.5. Processing a large adsorption dataset . . . . .	33
1.5.1. The NIST ISODB dataset . . . . .	33
1.5.2. A comparison between surface area calculation methods . . . . .	35
1.5.3. Variability of the dataset . . . . .	35
1.6. Conclusion . . . . .	38
Bibliography . . . . .	39
<b>2. Extending bulk analysis of porous compounds through calorimetry</b>	44
2.1. Introduction . . . . .	44
2.2. Thermodynamics of adsorption . . . . .	45
2.2.1. Energetic components of adsorption . . . . .	45

## Contents

2.2.2. The Gibbs surface excess approach . . . . .	45
2.2.3. Enthalpy of adsorption . . . . .	46
2.2.4. Measuring the enthalpy of adsorption . . . . .	46
2.3. Method . . . . .	47
2.3.1. Microcalorimetry . . . . .	47
2.4. Results and discussion . . . . .	48
2.4.1. Routine characterization of a MOF sample . . . . .	48
2.4.2. Analysis of a carbon sample for gas separation applications . . . . .	48
2.5. Conclusion . . . . .	50
Bibliography . . . . .	51
<b>3. Exploring the impact of synthesis and defects on adsorption measurements</b>	<b>49</b>
3.1. Introduction . . . . .	49
3.2. The defective nature of MOFs . . . . .	51
3.2.1. Types of crystal defects and their analogues in MOFs . . . . .	51
3.2.2. Consequences of defects . . . . .	53
3.2.3. Defect engineering of MOFs . . . . .	54
3.2.4. The propensity of UiO-66(Zr) for defect generation . . . . .	54
3.3. Materials and methods . . . . .	56
3.3.1. Materials . . . . .	56
3.3.2. Methods for quantifying defects . . . . .	58
3.4. Results and discussion . . . . .	59
3.4.1. Crystallinity of leached samples . . . . .	59
3.4.2. NMR . . . . .	59
3.4.3. Thermogravimetry results . . . . .	59
3.4.4. Nitrogen sorption at 77K . . . . .	62
3.4.5. Characterisation of trends . . . . .	62
3.4.6. Carbon dioxide isotherms . . . . .	68
3.5. Conclusion . . . . .	69
Bibliography . . . . .	70
<b>4. Exploring the impact of material form on adsorption measurements</b>	<b>78</b>
4.1. Introduction . . . . .	78
4.2. Shaping in context . . . . .	79
4.3. Materials, shaping and characterisation methods . . . . .	81
4.3.1. Materials . . . . .	81
4.3.2. Shaping Procedure . . . . .	82
4.3.3. Characterisation of powders and pellets . . . . .	82
4.3.4. Sample activation for adsorption . . . . .	83
4.4. Results and discussion . . . . .	83
4.4.1. Thermal stability . . . . .	83
4.4.2. Adsorption isotherms at 77K and room temperature . . . . .	83
4.4.3. Room temperature gas adsorption and microcalorimetry . . . . .	86

## *Contents*

4.4.4. Vapour adsorption . . . . .	92
4.5. Conclusion . . . . .	99
Bibliography . . . . .	100
<b>5. Exploring novel behaviours</b>	<b>104</b>
5.1. Introduction . . . . .	104
5.2. Literature . . . . .	104
5.3. Method . . . . .	104
5.4. Results and discussion . . . . .	104
5.5. Conclusion . . . . .	104
Bibliography . . . . .	105
<b>A. Common characterisation techniques</b>	<b>106</b>
A.1. Thermogravimetry . . . . .	106
A.2. Bulk density determination . . . . .	106
A.3. Skeletal density determination . . . . .	107
A.4. Nitrogen physisorption at 77 K . . . . .	107
A.5. Vapour physisorption at 298 K . . . . .	107
A.6. Gravimetric isotherms . . . . .	108
A.7. High throughput isotherm measuremnt . . . . .	108
A.8. Powder X-ray diffraction . . . . .	108
A.9. Nuclear magnetic resonance . . . . .	108
Bibliography . . . . .	108
<b>B. Synthesis method of referenced materials</b>	<b>109</b>
B.1. Takeda 5A reference carbon . . . . .	109
B.2. MCM-41 controlled pore glass . . . . .	109
B.3. Zr fumarate MOF . . . . .	109
B.4. UiO-66(Zr) for defect study . . . . .	109
B.5. UiO-66(Zr) for shaping study . . . . .	110
B.6. MIL-100(Fe) for shaping study . . . . .	110
B.7. MIL-127(Fe) for shaping study . . . . .	110
Bibliography . . . . .	111
<b>C. Appendix for chapter 4</b>	<b>112</b>
C.1. Calorimetry dataset UiO-66(Zr) . . . . .	112
C.2. Calorimetry MIL-100(Fe) . . . . .	113
C.3. Calorimetry MIL-127(Fe) . . . . .	116
Bibliography . . . . .	116
<b>D. Appendix for chapter 3</b>	<b>118</b>
D.1. Acid and solvent properties . . . . .	118
D.2. Powder diffraction patterns . . . . .	119

## *Contents*

D.3. TGA curves . . . . .	119
D.3.1. DMF leached samples . . . . .	119
D.3.2. Water leached samples . . . . .	120
D.3.3. Methanol leached samples . . . . .	121
D.3.4. DMSO leached samples . . . . .	122
D.3.5. High resolution curves . . . . .	123
D.4. Nitrogen sorption isotherms . . . . .	124
D.4.1. DMF leached samples . . . . .	124
D.4.2. H <sub>2</sub> O leached samples . . . . .	125
D.4.3. MeOH leached samples . . . . .	126
D.4.4. DMSO leached samples . . . . .	127
D.5. Characterisation . . . . .	128
Bibliography . . . . .	129

# 1. Building a framework for adsorption data processing

## 1.1. Introduction

Historically, the processing of isotherms was done by hand, with large worksheets being used for the calculations. As an example, we point out that one of the initial limitations of the Barrett-Joyner and Halenda method of determining pore size distribution was that each point had to be estimated with an approximation of critical pore radius, due to the tedious work involved in the calculation.<sup>(1)</sup>

The advent of computers meant that the calculations could be performed quickly and reliably and led to the introduction of more computationally demanding methods for isotherm processing, such as the DFT kernel fitting method for pore size distribution.<sup>(2,3)</sup> Commercial adsorption equipment which offers the users a complete software solution for any isotherm calculations is now commonplace and makes obtaining reports of desired properties for measured materials a matter of seconds.

Given the current ubiquitousness of adsorption as a characterisation method, particularly for investigating surfaces and porous compounds, there is a large pool of data published in the scientific community. Recent efforts have focused on building a database of adsorption isotherms<sup>(4)</sup>, to offer a searchable pool of standardised behaviours on different materials. This serves as both a useful reference for comparing synthesised compounds, as well as a method for quickly finding suitable materials which have the desired properties for a particular application.

The abundance of data reflects a trend in recent years where, due to the prevalence of digital records and cheap storage, more datapoints are available than ever before. As such, challenges now lie in making sense of the so called “big data”. Key performance indicators (KPI) such as specific surface area, working capacity and pore volume are commonly reported in scientific literature and used as benchmarking tools. Furthermore, several studies have attempted to find a reliable indicator for the suitability of an adsorbent for a specific application<sup>(5-7)</sup> such as pressure swing adsorption.

However, we feel that a critical step in the process has yet to be fully addressed. Transitioning from isotherms published in literature to the calculation of such KPIs requires individual implementation of previously mentioned techniques. As such, not only can errors arise in such implementations, but a critical survey of the results is tedious and time consuming. In conclusion, a standardised method of high throughput processing of such data would be invaluable not only for reference purposes, but also for in-depth studies of data reliability, structure-property relationships and effect of

## 1. Building a framework for adsorption data processing

variables on the adsorption properties of a material.

### Chapter summary

In this chapter an open-source software package is presented, which is released under an MIT licence and written in Python, intended to be used for manipulation, storage, visualisation and processing of adsorption isotherms. The software is aimed to give users a powerful yet easy to use package that can perform the kind of processing common to adsorption methodology, but using large datasets of hundreds or thousands of isotherms. The code is then used to process a dataset of 26000 isotherms from the NIST adsorption database in order to highlight the variability of adsorption data reported in literature on MOFs.

### Contribution

Paul Iacomi wrote the python code for the pyGAPS framework and is responsible for its publication and maintenance as an open source package. The IAST functionality is a modified version of the pylIAST code, published by Corey Simon. The data used in this chapter is available from the NIST Adsorption Database, maintained by Dan Siderius.

isotherms  
recoded  
by  
emily

## 1.2. Physical models of adsorption

As the process of characterisation of porous materials relies on mathematical models of how adsorption takes place inside the pores, this section details several such concepts.

A lot of effort was put into attempting to describe the phenomenon of adsorption. Through a well-defined model, the underlying mechanisms of adsorption can be understood. Unfortunately, the plethora of isotherm features and shapes can only be truly recreated by molecular simulation, which requires an exact knowledge of the adsorbent structure and its interaction with the guest molecules. Nevertheless, simple models derived from a kinetic or thermodynamic view of adsorption can be useful for obtaining simple parameters which are representative of physical factors such as guest-host interaction, surface area, pore size, and total capacity.

Isotherm models which have a thermodynamical basis are derived from the Gibbs equation (Equation 1.1). This approach describes adsorption in terms of a surface excess with respect to the bulk gas phase. The pressure and volume concepts of the bulk phase are replaced by the 2-dimensional analogues of spreading pressure ( $\pi$ ) and surface area.

$$\left( \frac{d\pi}{d \ln p} \right) = \frac{n}{A} R_g T \quad (1.1)$$

By substituting spreading pressure with an equation of state for the adsorbed phase, an expression for the amount adsorbed can be obtained as a function of bulk phase

## 1. Building a framework for adsorption data processing

pressure. Models which are derived from this equation include Henry's law, the virial model and vacancy solution theory.

Adsorption can also be described a kinetic standpoint, where the rate of adsorption and desorption of molecules on available sites is mathematically modelled. Equations based on kinetics include the Langmuir model, the BET model the Temkin model and empirical or semi-empirical derivatives such as the Toth, Quadratic or the Jensen-Seaton model A page of figures for different models and how the described isotherm varies with different values of their parameters can be seen in Figure 1.1. The following section will describe these equations, together with their assumptions and applicability.

### 1.2.1. The Henry model

The simplest method of describing adsorption on a surface is Henry's law. It assumes only interactions with the adsorbate surface and is described by a linear dependence of adsorbed amount with increasing pressure.

$$n_a(p) = K_H p \quad (1.2)$$

It is derived from the Gibbs isotherm, by substituting a two dimensional analogue to the ideal gas law. From a physical standpoint, Henry's law is unrealistic as adsorption sites will saturate at higher pressures. However, the constant  $K_H$ , or Henry's constant, can be thought of as a measure of the strength of the interaction of the probe gas with the surface. At very low concentrations of gas there is a theoretical requirement for the applicability of Henry's law. Therefore, most models reduce to Equation 1.2 as  $\lim_{p \rightarrow 0} n(p)$ .

### 1.2.2. Langmuir and multi-site Langmuir model

The Langmuir theory<sup>(8)</sup>, proposed at the start of the 20th century, states that adsorption takes place on specific sites on a surface, until all sites are occupied. It is derived from a kinetic model of gas adsorption and is based on several assumptions.

- All sites are equivalent and have the same chance of being occupied.
- Each adsorbate molecule can occupy one adsorption site.
- There are no interactions between adsorbed molecules.
- The rates of adsorption and desorption are proportional to the number of sites currently free and currently occupied, respectively.
- Adsorption is complete when all sites are filled.

## 1. Building a framework for adsorption data processing

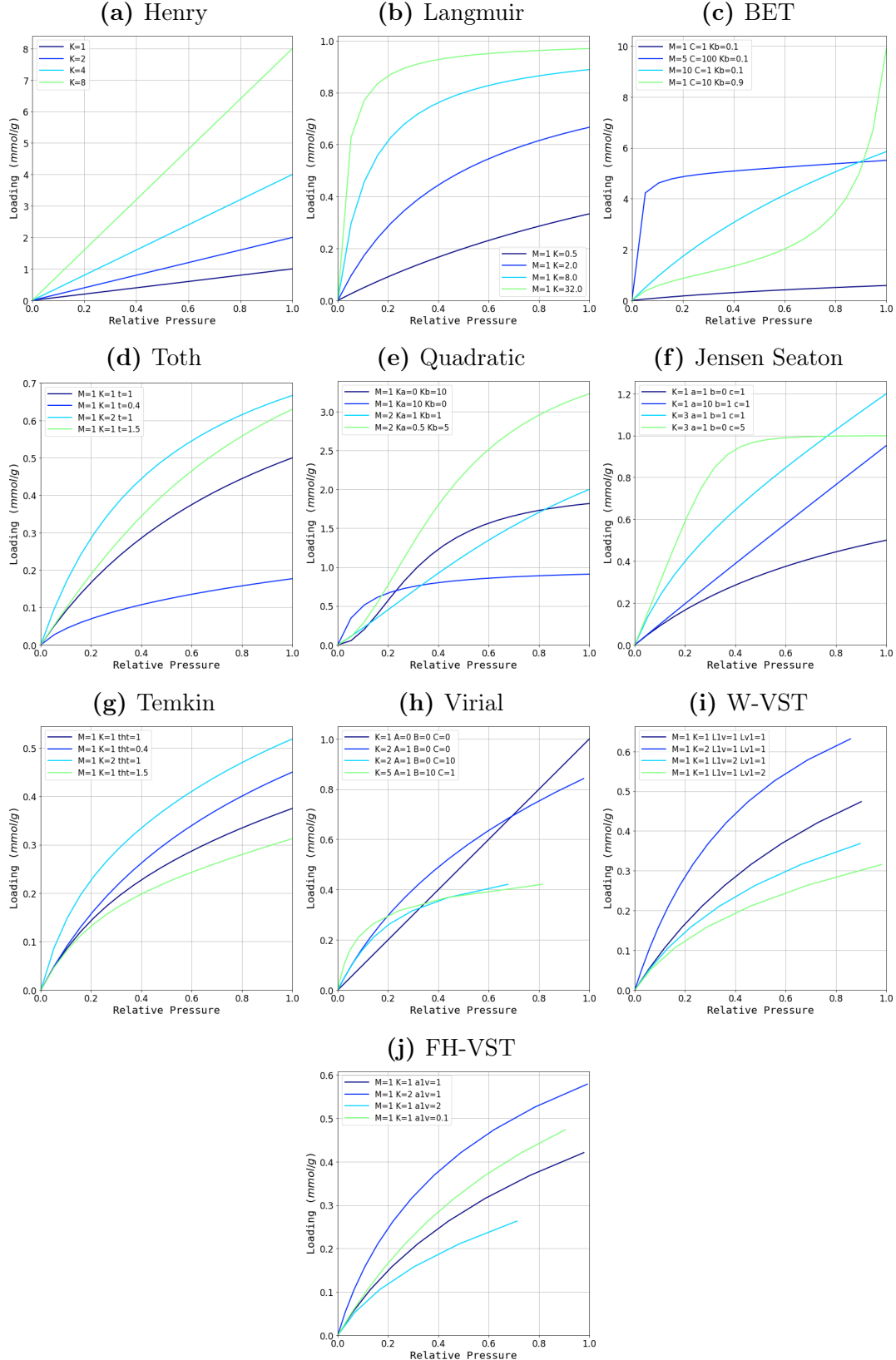


**Figure 1.1.:** The various adsorption models discussed in this chapter, alongside the influence of their parameters on the resulting isotherm.

## 1. Building a framework for adsorption data processing

Using these assumptions we can define rates for both adsorption and desorption. The adsorption rate (Equation 1.3) will be proportional to the number of sites available on the surface, as well as the number of molecules in the gas, which is given by pressure. The desorption rate, on the other hand, will be proportional to the number of occupied sites and the energy of adsorption (Equation 1.4). It is also useful to define  $\theta = n_a/n_a^m$  as the surface coverage, the number of sites occupied divided by the total sites. At equilibrium, the rate of adsorption and the rate of desorption are equal, therefore the two equations can be combined. The equation can then be arranged to obtain an expression for the loading called the Langmuir model (Equation 1.7).

$$v_a = k_a p (1 - \theta) \quad (1.3)$$

$$v_d = k_d \theta \exp\left(-\frac{E_{ads}}{RT}\right) \quad (1.4)$$

$$v_a = v_d \quad (1.5)$$

$$k_a p (1 - \theta) = k_d \theta \exp\left(-\frac{E_{ads}}{RT}\right) \quad (1.6)$$

$$n_a(p) = n_a^m \frac{Kp}{1 + Kp} \quad (1.7)$$

The Langmuir constant  $K$  is the product of the individual desorption and adsorption constants  $k_a$  and  $k_d$  and exponentially related to the energy of adsorption  $E_{ads}$ .

A common extension to the Langmuir model is to consider the experimental isotherm to be the sum of several Langmuir-type isotherms, each with specific maximum coverage and affinities. The underlying assumption is that the adsorbent has several distinct types of homogeneous adsorption sites and a Langmuir equation is used for each. This is particularly applicable in cases where the structure of the adsorbent suggests that different types of sites are present, such as in crystalline materials of variable chemistry like zeolites and MOFs. The resulting isotherm equation becomes:

$$n_a(p) = \sum_i n_{a,i}^m \frac{K_i p}{1 + K_i p} \quad (1.8)$$

In practice, only up to three adsorption sites are usually considered.

### 1.2.3. BET model

Like the Langmuir mode, The BET model<sup>(9)</sup> assumes that adsorption is kinetically driven and takes place on adsorption sites at the material surface. However, each adsorbed molecule becomes, in itself a secondary adsorption site, such that incremental layers are formed. The conditions imagined by the BET model are:

- The surface adsorption sites are equivalent, and therefore the surface is considered heterogeneous.

## 1. Building a framework for adsorption data processing

- There are no lateral interactions between adsorbed molecules.
- The adsorption occurs in layers, with adsorbed molecules acting as sites for the next layer.

A percentage of the surface  $\theta_x$  is occupied with  $x$  layers. For each layer at equilibrium, the adsorption and desorption rates must be equal. The Langmuir model is then applied for each of layer as shown in Table 1.1. It is assumed that the adsorption energy of a molecule on the second and higher layers is just the condensation energy of the adsorbent  $E_{i>1} = E_L$ . Since it follows that all layers beside the first have the same properties, we can also define  $g = k_{d_2}k_{a_2} = k_{d_3}k_{a_3} = \dots$ .

**Table 1.1.:** Derivation of the BET method from each adsorbed layer

All layers	Re-arranged
$k_{a_1}p\theta_0 = k_{d_1}\theta_1 \exp\left(-\frac{E_1}{RT}\right)$	$p\theta_0 = \frac{k_{d_1}}{k_{a_1}}\theta_1 \exp\left(-\frac{E_1}{RT}\right)$
$k_{a_2}p\theta_1 = k_{d_2}\theta_2 \exp\left(-\frac{E_2}{RT}\right)$	$p\theta_1 = g\theta_2 \exp\left(-\frac{E_L}{RT}\right)$
$k_{a_2}p\theta_2 = k_{d_3}\theta_3 \exp\left(-\frac{E_3}{RT}\right)$	$p\theta_2 = g\theta_3 \exp\left(-\frac{E_L}{RT}\right)$
$\vdots$	$\vdots$
$k_{a_i}p\theta_{i-1} = k_{d_i}\theta_i \exp\left(-\frac{E_i}{RT}\right)$	$p\theta_{i-1} = g\theta_i \exp\left(-\frac{E_L}{RT}\right)$

The coverage for each layer  $\theta$  can now be expressed in terms of  $\theta_0$ .

$$\theta_i = \left[ p \frac{k_{a_1}}{k_{d_1}} \exp\left(-\frac{E_1}{RT}\right) \right] x^{i-1} \theta_0 \quad (1.9)$$

where

$$x = \frac{p}{g} \exp\left(-\frac{E_L}{RT}\right) \quad (1.10)$$

A constant C may be defined such that:

$$C = \frac{k_{a_1}}{k_{d_1}} g \exp\left(\frac{E_1 - E_L}{RT}\right) \quad (1.11)$$

$$\theta_i = C x^i \theta_0 \quad (1.12)$$

For all the layers, the equations can be summed:

## 1. Building a framework for adsorption data processing

$$\frac{n}{n_m} = \sum_{i=1}^{\infty} i\theta^i = C \sum_{i=1}^{\infty} ix^i \theta_0 \quad (1.13)$$

and since

$$\theta_0 = 1 - \sum_1^{\infty} \theta_i \sum_{i=1}^{\infty} ix^i = \frac{x}{(1-x)^2} \quad (1.14)$$

Then we obtain the BET equation:

$$n_a(p) = n_a^m \frac{C(p/p_0)}{(1-p/p_0)[1-(p/p_0)+C(p/p_0)]} \quad (1.15)$$

The BET constant  $C$  is exponentially proportional to the difference between the surface adsorption energy and the intermolecular attraction and can be seen to influence the “knee” a BET-type isotherm has at low pressure, before statistical monolayer formation.

### 1.2.4. Toth model

The Toth model is an empirical modification to the Langmuir equation (Equation 1.7) which introduces a power parameter for the denominator leading to the following equation:

$$n_a(p) = n_a^m \frac{Kp}{[1+(Kp)^t]^{1/t}} \quad (1.16)$$

The parameter  $t$  is a measure of the system heterogeneity. Thanks to this additional parameter, the Toth equation can accurately describe a large number of adsorbent/adsorbate systems and, due to its correct behaviour in both the low and high pressure limits, is recommended as the fitting isotherms of many adsorbents such as hydrocarbons, carbon oxides, hydrogen sulphide and alcohols on activated carbons and zeolites.

### 1.2.5. Temkin model

The Temkin adsorption isotherm<sup>(10)</sup>, like the Langmuir model, considers a surface with  $n_a^m$  identical adsorption sites, but takes into account adsorbate-adsorbate interactions by assuming that the heat of adsorption is a linear function of coverage. The formula in Equation 1.17 is derived using a mean-field argument and uses an asymptotic approximation to obtain an explicit equation for the loading.<sup>(11)</sup>

$$n_a(p) = n_a^m \frac{Kp}{1+Kp} + n_a^m \theta \left( \frac{Kp}{1+Kp} \right)^2 \left( \frac{Kp}{1+Kp} - 1 \right) \quad (1.17)$$

## 1. Building a framework for adsorption data processing

Here,  $n_a^m$  and K have the same physical meaning as in the Langmuir model. The additional parameter  $\theta$  describes the strength of the adsorbate-adsorbate interactions ( $\theta < 0$  for attractions).

### 1.2.6. Jensen-Seaton model

When modelling supercritical adsorption in micropores, a requirement was highlighted by Jensen and Seaton in 1996<sup>(12)</sup> that at sufficiently high pressures the adsorption isotherm should not reach a horizontal plateau corresponding to saturation but that this asymptote should continue to rise due to the compression of the adsorbate in the pores. They developed a semi-empirical equation to describe this phenomenon based on a function that interpolates between two asymptotes: the Henry's law asymptote at low pressure and an asymptote reflecting the compressibility of the adsorbate at high pressure.

$$n(p) = K_H p \left(1 + \frac{K_H p}{[a(1+bp)]^c}\right)^{(-1/c)} \quad (1.18)$$

Here  $K_H$  is the Henry constant,  $b$  is the compressibility of the adsorbed phase and  $c$  an empirical constant.

The equation can be used to model both absolute and excess adsorption as the pore volume can be incorporated into the definition of  $b$ , although this can lead to negative adsorption slopes for the compressibility asymptote. This equation has been found to provide a better fit for experimental data from microporous solids than the Langmuir or Toth equation, in particular for adsorbent/adsorbate systems with high Henry's constants where the amount adsorbed increases rapidly at relatively low pressures and then slows down dramatically.

### 1.2.7. Quadratic model

The quadratic adsorption isotherm<sup>(13)</sup> exhibits an inflection point. The loading is convex at low pressures but changes concavity as it saturates, yielding an S-shape. The S-shape can be explained by adsorbate-adsorbate attractive forces: the initial convexity is due to a cooperative effect of adsorbate-adsorbate attractions aiding in the recruitment of additional adsorbate molecules.

$$n(p) = n_a^m \frac{(K_a + 2K_bp)p}{1 + K_{ap} + K_{bp}^2} \quad (1.19)$$

The parameter  $K_a$  can be interpreted as the Langmuir constant; the strength of the adsorbate-adsorbate attractive forces is embedded in  $K_b$ . It is often useful in systems where the energy of guest-guest interactions is actually higher than the energy of adsorption, such as when adsorbing water on a hydrophobic surface.

### 1.2.8. Virial model

A virial isotherm model attempts to fit the measured data to a factorized exponent relationship between loading and pressure.<sup>(14)</sup>

$$p = n \exp (K_1 n^0 + K_2 n^1 + K_3 n^2 + K_4 n^3 + \dots + K_i n^{i-1}) \quad (1.20)$$

It has been applied with success to describe the behaviour of standard as well as supercritical isotherms. The factors are usually empirical, although some relationship with physical properties can be determined: the first constant is related to the Henry constant at zero loading, while the second constant is a measure of the interaction strength with the surface.

$$K_1 = -\ln K_{H,0} \quad (1.21)$$

In practice, besides the first constant, only 2–3 factors are used.

### 1.2.9. Vacancy solution theory models

The vacancy solution theory (VST) family of models, are based on the concept of a “vacancy” species and assume that the adsorbed phase is analogous to a mixture of vacancies and the adsorbate. The main assumptions in the VST models are defined as follows:

- A vacancy is an imaginary entity defined as a vacuum space, which acts as the solvent in both the gas and adsorbed phases.
- The properties of the adsorbed phase are defined through the Gibbs approach, as excess properties in relation to a dividing surface.
- The entire system, including the adsorbent, is at thermal equilibrium. However, only the gas and the adsorbed phases are in thermodynamic equilibrium.
- The equilibrium of the system is maintained by the spreading pressure which arises from a potential field at the surface.

It is possible to derive expressions for the vacancy chemical potential in both the adsorbed phase and the gas phase, which when equated give the following equation of state for the adsorbed phase:

$$\pi = -\frac{R_g T}{\sigma_v} \ln y_v x_v \quad (1.22)$$

Here  $y_v$  is the activity coefficient and  $x_v$  is the mole fraction of the vacancy in the adsorbed phase. This can then be introduced into the Gibbs equation (Equation 1.1) to

## 1. Building a framework for adsorption data processing

obtain a general isotherm equation for VST-type models (Equation 1.23) where  $K_H$  is the Henry's constant and  $f(\theta)$  is a function that describes the non-ideality of the system in terms of activity coefficients of the adsorbate and vacancy species.

$$p = \frac{n_{ads}}{K_H} \frac{\theta}{1-\theta} f(\theta) \quad (1.23)$$

The general VST equation requires an expression for the activity coefficients  $f(\theta)$ . One option is to use the Wilson<sup>(15)</sup> approach, which expresses the activity coefficient in terms of the mole fractions of the two species (adsorbate and vacancy) and two constants  $\Lambda_{1v}$  and  $\Lambda_{1v}$ . The equation then for activity coefficients becomes:

$$f(\theta) = \Lambda_{1v} \frac{1 - (1 - \Lambda_{1v})\theta}{\Lambda_{1v} + (1 - \Lambda_{1v})\theta} \exp \left( - \frac{\Lambda_{1v}(1 - \Lambda_{1v})\theta}{1 - (1 - \Lambda_{1v})\theta} - \frac{(1 - \Lambda_{1v})\theta}{\Lambda_{1v} + (1 - \Lambda_{1v})\theta} \right) \quad (1.24)$$

A simpler alternative was introduced by Cochran.<sup>(16)</sup> The result is a three parameter equation based on the Flory–Huggins equation for the activity coefficient.  $f(\theta)$  is represented as

$$f(\theta) = \exp \frac{\alpha_{1v}^2 \theta}{1 + \alpha_{1v} \theta} \quad \text{where} \quad \alpha_{1v} = \frac{\alpha_1}{\alpha_v} - 1 \quad (1.25)$$

Here  $\alpha_1$  and  $\alpha_v$  are the molar areas of the adsorbate and the vacancy respectively. Both the Wilson and Flory–Huggins expressions for the vacancy-adsorbate interactions can be directly inserted in the general VST model (Equation 1.23).

## 1.3. Characterisation of materials through adsorption

Adsorption is a powerful tool for characterisation of materials. As it can give insight into the surface properties of solids, it is most often used for the investigation of porous or finely divided materials where the surface area to volume ratio is high enough for adsorption to be detected with common laboratory measurement techniques such as manometry and gravimetry (see Appendix A). The most common properties which can be obtained through adsorption methods are probe accessible surface area, pore volume and pore size distribution. Other characteristics such as surface chemistry or material response can be probed through adsorption. Finally, pure component adsorption isotherms can be used to predict multicomponent adsorption through computational models such as IAST. The following section will go into detail on how such methods are applied.

### 1.3.1. Specific surface area and pore volume calculation

#### BET surface area

The BET method<sup>(9)</sup> for determining surface area is the recommended IUPAC method<sup>(17)</sup> to calculate the surface area of a porous material. It is generally applied on isotherms

## 1. Building a framework for adsorption data processing

obtained through N<sub>2</sub> adsorption at 77 K, although other adsorbates (Ar at 77 K or 87 K, Kr at 77 K, CO<sub>2</sub> at 293 K) have been used. In principle, any probe with an adsorption isotherm which can be described through the BET equation in the low pressure regime can be used.

As previously mentioned, subsection 1.2.3 the BET model assumes that adsorption takes place in incremental layers on the material surface. Even if the adsorbent is porous, the initial amount adsorbed (usually between 0.05–0.4  $p/p_0$ ) can be described through the equation written in its linear form:

$$\frac{p/p_0}{n_{ads}(1 - p/p_0)} = \frac{1}{n_m C} + \frac{C - 1}{n_m C} (p/p_0) \quad (1.26)$$

If a plot of the isotherm points as  $(p/p_0)/n_{ads}(1 - p/p_0)$  versus  $p/p_0$  is generated, a linear region can usually be found. The slope and intercept of this line can then be used to calculate  $n_m$ , the amount adsorbed at the statistical monolayer, as well as  $C$ , the BET constant.

$$n_m = \frac{1}{s + i} \quad C = \frac{s}{i} + 1 \quad (1.27)$$

From the BET monolayer capacity, the specific surface area can be calculated if the area taken up by one of the adsorbate molecules on the surface is known. The calculation uses the following equation together with Avogadro's number:

$$a_{BET} = n_m A_N \sigma \quad (1.28)$$

While commonly used for surface area determination, the BET area should be used with care, as the assumptions made in its calculation may not hold. To augment the validity of the BET method, Rouquerol<sup>(18)</sup> proposed several checks to ensure that the selected BET region is valid:

- The BET ( $C$ ) obtained should be positive;
- In the corresponding Rouquerol plot where  $n_{ads}(1 - p/p_0)$  is plotted with respect to  $p/p_0$ , the points chosen for BET analysis should be strictly increasing;
- The loading at the statistical monolayer should be situated within the limits of the BET region.

Regardless, the BET surface area should still be interpreted carefully. Since adsorption takes place on the pore surface, microporous materials which have pores of similar or smaller size as the probe molecule used will not give a realistic surface area. In the micropore range it is difficult to separate pore condensation behaviour from multilayer adsorption. Furthermore, the cross-sectional area of the molecule on the surface cannot be guaranteed. For example, nitrogen has been known to adopt a different conformation on the surface of some materials due to inter-molecular forces, which effectively lowers its cross-sectional area.<sup>(18)</sup>

## 1. Building a framework for adsorption data processing

### Langmuir surface area

The Langmuir equation (Equation 1.7) can be also be expressed in a linear form by rearranging it as:

$$\frac{p}{n} = \frac{1}{Kn_m} + \frac{p}{n_m} \quad (1.29)$$

Assuming the data can be fitted with a Langmuir model, by plotting  $p/n$  against pressure, a straight line will be obtained. The slope and intercept of this line can then be used to calculate  $n_m$ , the amount adsorbed at the monolayer capacity, as well as  $K$ , the Langmuir constant.

$$n_m = \frac{1}{s} \quad K = \frac{1}{i * n_m} \quad (1.30)$$

The surface area can then be calculated by using the monolayer capacity in a manner analogous to the BET surface area method.

$$a_{Langmuir} = n_m A_N \sigma \quad (1.31)$$

The Langmuir method for determining surface area assumes that adsorption takes place until all active sites on the material surface are occupied, or until monolayer formation in the case of complete surface coverage. As most adsorption processes (except chemisorption) don't follow this behaviour, it is important to regard the Langmuir surface area as an estimate.

### Ideal isotherms or thickness functions

The initial part of an isotherm (the Henry regime) can be seen to be very dependent on the interactions between the adsorbate and the surface. However, subsequent layers are less influenced by the material and can often be assumed, like in the BET model, to have an energy of adsorption identical to the enthalpy of liquefaction of the bulk liquid. Therefore, their formation will essentially depend only on partial pressure.

With this assumption, several studies have been focused on obtaining an “ideal” isotherm of adsorption on a non-porous material which can then, if the cross-sectional area of the molecule is known, be transformed in a function capable of predicting the thickness of the adsorbed layer as a function of pressure. This kind of empirical function, also referred to as a *thickness function* or *t-curve*, can be used as an alternative method for surface area determination, as explained in the following section. These curves are also used in the classical methods for calculating mesoporous size distribution. It is important to clarify that the function is only applicable for a single adsorbent and temperature.

## 1. Building a framework for adsorption data processing

For example, two common thickness functions applicable for nitrogen at 77 K are the Halsey<sup>(19)</sup> (Equation 1.32) and the Harkins and Jura<sup>(20)</sup> (Equation 1.33) curves.

$$t_{Halsey} = 0.354 \left( \frac{-5}{\log(p/p_0)} \right)^{1/3} \quad (1.32)$$

$$t_{Harkins\&Jura} = \left( \frac{0.1399}{0.034 - \log_{10}(p/p_0)} \right)^{1/2} \quad (1.33)$$

### t-plot method

The t-plot method is an empirical method developed as a tool to determine the surface area of porous materials, which can also be used for other calculations, such as external surface area and pore volume.<sup>(21)</sup> A plot is constructed, where the isotherm loading data is plotted versus the ideal thickness of the adsorbate layer, obtained through a t-curve (section 1.3.1). It stands to reason that, in the case when the experimentally measured isotherm conforms to the model, a straight line will be obtained with its intercept through the origin. However, as in most cases there are differences between adsorption in pores and surface multilayer adsorption, the t-plot will deviate and reveal features which can be analysed to obtain material characteristics. For example, a sharp vertical deviation will indicate condensation in a type of mesopore while a gradual slope will indicate adsorption on a specific surface.

The slope of a linear section can be used to calculate the area where adsorption is taking place. If the linear region occurs at low loadings, it will represent the total surface area of the material. If at the end of the curve, it will instead represent adsorption on external surface area. The formula to calculate an area starting from the t-plot slope is presented in Equation 1.34, where  $\rho_l$  is the liquid density of the adsorbate at experimental conditions.

$$a_{surface} = \frac{sM_m}{\rho_l} \quad (1.34)$$

If the linear region selected is after a vertical deviation, the intercept of the calculated line will no longer pass through the origin. This intercept can be used to calculate the volume of the filled pore through the following equation:

$$V_{ads} = \frac{iM_m}{\rho_l} \quad (1.35)$$

As the t-plot method compares the experimental isotherm with an ideal model, care must be taken to ensure that the t-curve is an accurate representation of the thickness of the adsorbate layer. Since there is no such thing as a universal thickness curve, a reliable model which is applicable to both material and adsorbate should be chosen. It should also be noted that, features on the t-plot found at loadings lower than the monolayer thickness may not have any physical meaning.

## 1. Building a framework for adsorption data processing

### $\alpha_s$ Method

In order to extend the t-plot analysis with other adsorbents and non-standard thickness curves, the  $\alpha_s$  method was devised.<sup>(22)</sup> Instead of attempting to find an ideal isotherm that describes the thickness of the adsorbed layer, a reference isotherm is used. This isotherm is measured on a non-porous version of the same material, which is assumed to have identical surface characteristics. The dimensionless  $\alpha_s$  values are obtained from this isotherm by dividing the loading values by the amount adsorbed at a specific relative pressure, usually taken as  $p/p_0 = 0.4$  since nitrogen hysteresis loops theoretically close at this point.

$$\alpha_s = \frac{n_a}{n_{0.4}} \quad (1.36)$$

The analysis then proceeds as in the t-plot method, with the same explanation for observed features. The only difference is that the surface area calculation from linear regions observed uses the known specific area of the reference material.

$$A = \frac{sA_{ref}}{(n_{ref})_{0.4}} \quad (1.37)$$

The reference isotherm chosen for the  $\alpha_s$  method must be a description of adsorption on a completely non-porous sample of the same material. It is often impossible to obtain such a version. Furthermore, an adsorption isotherm on a non-porous solid may be a challenging endeavour, due to the small ratio of surface area to volume.

### 1.3.2. Assessing porosity

Characterization of pore sizes and their distribution in a porous material is often the main goal when performing adsorption experiments. When it comes to such materials, three kinds of pore sizes can be defined, based on their lengthscale: micropores ( $<2\text{ nm}$ ), mesopores ( $2\text{ nm}$  to  $50\text{ nm}$ ), and macropores ( $>50\text{ nm}$ ).

Macropores are generally unable to be characterised through adsorption, with methods such as mercury intrusion porosimetry as the standard for pore size determination at this lengthscale, although other alternatives have been suggested<sup>(23)</sup> due to the high toxicity of mercury.

In the mesopore range, “classical” methods are often used, which are based on the application of Kelvin’s equation pertaining to capillary condensation. This equation calculates the critical pressure at which the fluid completely files a pore of a specific diameter. It is applicable to a range of geometries is used in multiple approaches such as the Barrett-Joyner-Halenda (BJH) method or the Dollimore-Heal (DH) method.

For microporous materials, the Kelvin equation, with its assumption of continuous fluid properties and comparable density of the adsorbed state to bulk liquid density breaks down. An atomistic approach is required, addressing the interaction between

## 1. Building a framework for adsorption data processing

solid-fluid and fluid-fluid through potential functions. The Horvath-Kawazoe or HK method is often used, alongside the older Dubinin-Radushkevich model.

Finally, computational methods based on Grand Canonical Monte Carlo (GCMC) and density functional theory (DFT) together with its derivations such as non-local DFT (NLDFT) and quenched solid state DFT (QSDFT) should be mentioned, as they can be used for multiscale (micropore and mesopore) characterisation. These methods rely on *in-silico* simulation of isotherms on a range of pore sizes, which can then be collated in a so-called *kernel*, able to be used to deconvolute an experimental isotherm to obtain a pore size distribution.

It should be noted that all methods here described require knowledge of the pore geometry and depend on the material having pores which conform to a well-defined shape. Real adsorbents usually have interconnected networks of irregular pores, which the ideal pores used in these models merely approximate.

### Mesoporous size distribution

**The Kelvin equation** Since the Kelvin equation is the basis of most mesoporous PSD calculations, such as the BJH and DH methods, it will be described first. The original form of the equation (Equation 1.38) gives the dependence of pressure on the radius of curvature of a meniscus in a pore  $r$  by means of surface tension  $\gamma$ , molar liquid volume, here expressed as  $v_l = M_m/\rho_l$  and the fluid contact angle with the surface  $\theta$ . The fluid is often assumed to be fully wetting, with  $\theta = 0$  and  $\cos \theta = 1$ .

$$\ln\left(\frac{p}{p_0}\right) = -\frac{\gamma M_m}{\rho_l RT} \frac{2 \cos \theta}{r} \quad (1.38)$$

To apply the Kelvin equation to different types of pore systems, the generalized form presented in Equation 1.39 is used. It replaces the meniscus radius by a mean radius of curvature  $r_m$ .

$$\ln\left(\frac{p}{p_0}\right) = -\frac{\gamma M_m}{\rho_l RT} \frac{2}{r_m} \quad (1.39)$$

The mean radius of curvature is defined through the two principal radii of the curved interface.

$$\frac{1}{r_m} = \frac{1}{2} \left( \frac{1}{r_1} + \frac{1}{r_2} \right) \quad (1.40)$$

The relationship of the kelvin radius  $r_m$  to the actual pore radius is more subtle, as it depends on pore geometry and the filling state of the pore.<sup>(24)</sup> If considering a cylindrical pore open at both ends, the radius reduces to the original Kelvin equation during the desorption phase, and takes other values with different combinations of parameters as can be seen in Table 1.2.

According to Rouquerol<sup>(18)</sup>, in adopting this approach, it is assumed that:

## 1. Building a framework for adsorption data processing

**Table 1.2.:** Assumed relationship between pore geometry and meniscus geometry during adsorption and desorption

Pore geometry	Assumed meniscus geometry	
	Adsorption	Desorption
infinite slit	infinite radius cylindrical	concave
open-ended cylinder	cylindrical	spherical
sphere	spherical	spherical

- The Kelvin equation is applicable over the pore range (mesopores). Therefore in pores which are below a certain size (around 2.5 nm), the granularity of the liquid-vapour interface becomes too large for classical bulk methods to be applied.
- The meniscus curvature is controlled by pore size and shape. Ideal shapes for the curvature are assumed.
- Pores are rigid and of well defined shape. Their geometry is considered to be invariant across the entire adsorbate.
- The filling/emptying of each pore does not depend on its location.
- Adsorption on the pore walls is not different from surface adsorption.

**The Barrett, Joyner and Halenda (BJH) method** The BJH method for calculating pore size distribution is based on a classical description of the adsorbate behaviour in the adsorbent pores.<sup>(1)</sup> Under this method, the guest is adsorbing on the pore walls following an ideal model, and decreasing the apparent pore volume until condensation takes place, filling the entire pore. The critical radius is a sum of two radii, the adsorbed layer thickness, which can be modelled by a thickness model (such as Halsey, Harkins & Jura or similar as presented in section 1.3.1) and a critical radius model for condensation/evaporation, based on a form of the Kelvin equation.

$$r_p = t + r_k \quad (1.41)$$

The original model uses the desorption curve as a basis for calculating pore size distribution. Between two points of the curve, the volume desorbed can be described as the volume contribution from pore evaporation and the volume from layer thickness decrease as per Equation 1.41. The computation is done cumulatively, starting from the filled pores and calculating the volume adsorbed in a pore for each point using the following equation:

$$V_p = \left( \frac{\bar{r}_p}{\bar{r}_k + \Delta t_n} \right)^2 \left( \Delta V_n - \Delta t_n \sum_{i=1}^{n-1} \Delta A_p + \Delta t_n \bar{t}_n \sum_{i=1}^{n-1} \frac{\Delta A_p}{\bar{r}_p} \right) \quad (1.42)$$

## 1. Building a framework for adsorption data processing

where

$$A = 2\Delta V_p / r_p \quad (1.43)$$

In the BJH equation:

- $\Delta A_p$  is the area of the pores
- $\Delta V_p$  is the adsorbed volume change between two points
- $\bar{r}_p$  is the average pore radius calculated as a sum of the kelvin radius and layer thickness of the pores at pressure p between two measurement points
- $\bar{r}_k$  is the average kelvin radius between two measurement points
- $\bar{t}_n$  is the average layer thickness between two measurement points
- $\Delta t_n$  is the average change in layer thickness between two measurement points

Then, by plotting  $\Delta V/(2 * \Delta r_p)$  versus the width of the pores calculated for each point, the pore size distribution can be obtained.

**The Dollimore-Heal (DH) method** The DH or Dollimore-Heal method<sup>(25)</sup> is an extension of the BJH method which takes into account the geometry of the pores by introducing a length component. Like the BJH method, it is based on a classical description of the adsorbate behaviour in the adsorbent pores and uses the same assumptions. The modified equation becomes:

$$V_p = \left( \frac{\bar{r}_p}{\bar{r}_k + \Delta t_n} \right)^2 \left( \Delta V_n - \Delta t_n \sum_{i=1}^{n-1} \Delta A_p + 2\pi \Delta t_n \bar{t}_n \sum_{i=1}^{n-1} L_p \right) \quad (1.44)$$

$$A = 2\Delta V_p / r_p \quad (1.45)$$

$$L = \Delta A_p / 2\pi r_p \quad (1.46)$$

The meaning of each symbol is the same as in the BJH equation. As before, a plot of  $\Delta V/(2 * \Delta r_p)$  versus the width of the pores calculated for each point yields the pore size distribution. The Dollimore-Heal method is used on the desorption branch, of the isotherm but often also applied on the adsorption branch.

## Microporous size distribution

When it comes to micropores (width < 2 nm), classical fluid methods stop being viable. Adsorption of molecules in these pores of comparable scale is highly dependent on the surface properties and on guest-host interaction and leads to adsorbate phase densities which are often very different than those in the bulk liquid state. In order to model adsorption in such pores, a good description of both solid-fluid and fluid-fluid potential functions is required.

## 1. Building a framework for adsorption data processing

**The Horvath-Kawazoe (HK) method** The H-K method attempts to describe the adsorption within pores by calculation of the average potential energy for a pore.<sup>(26)</sup> The method starts by assuming the relationship between the gas phase as being:

$$R_g T \ln \left( \frac{p}{p_0} \right) = U_0 + P_a \quad (1.47)$$

Here  $U_0$  is the potential function describing the surface to adsorbent interactions and  $P_a$  is the potential function describing guest-guest interactions. This equation is derived from the equation of the free energy of adsorption at constant temperature where the term  $T\Delta S^{tr}(w/w_\infty)$  is assumed to be negligible.

If it is assumed that a Lennard-Jones-type potential function can accurately describe the interactions between adsorbate and surface molecules, then the two contributions to the total potential can be replaced by the extended function in Equation 1.48.

$$\begin{aligned} RT \ln(p/p_0) &= N_A \frac{n_a A_a + n_A A_A}{2\sigma^4(l-d)} \\ &\times \int_{d/2}^{1-d/2} \left[ -\left(\frac{\sigma}{r}\right)^4 + \left(\frac{\sigma}{r}\right)^{10} - \left(\frac{\sigma}{l-r}\right)^4 + \left(\frac{\sigma}{l-r}\right)^{10} \right] dx \end{aligned} \quad (1.48)$$

Here  $l$  is the width of the pore,  $d$  defined as  $d = d_a + d_A$  is the sum of the diameters of the adsorbate and adsorbent molecules,  $n_a$  is number of molecules of adsorbent and  $A_a$  and  $A_A$  the Lennard-Jones potential constant of the fluid molecule and solid molecule respectively. They are defined as

$$A_a = \frac{6mc^2\alpha_a\alpha_A}{\alpha_a/\kappa_a + \alpha_A/\kappa_A} \quad (1.49)$$

and

$$A_a = \frac{3mc^2\alpha_A\kappa_A}{2} \quad (1.50)$$

Where  $m$  is the mass of an electron,  $\alpha_a$  and  $\alpha_A$  are the polarizability of the adsorbate and adsorbent molecule and  $\kappa_a$  and  $\kappa_A$  the magnetic susceptibility of the adsorbate molecule and adsorbent molecule, respectively.

The HK method is applicable to slit pores, and it can be extended through modification to cylindrical and spherical pores. It is worth noting that there are several assumptions which limit its applicability.

- The HK method is reliant on knowledge of the properties of the surface atoms. This assumption is true only if the material surface is homogenous. Furthermore, longer range interactions with multiple surface layers are not considered.

## 1. Building a framework for adsorption data processing

- Each pore is modelled as uniform and of infinite length. Materials with varying pore shapes or highly interconnected networks may not give realistic results.
- Only dispersive forces are accounted for. If the adsorbate-adsorbent interactions have other specific contributions, as is the case for dipole-dipole or *pi*-backbonding interactions, the Lennard-Jones potential function will not be an accurate description.
- The model does not have a description of capillary condensation. This means that the pore size distribution can only be considered accurate up to a maximum of 3 nm to 5 nm.

### Multiscale computational methods

DFT theory emerged as a rigorous description of molecular adsorption in pores.<sup>(2)</sup> It calculates the properties of the fluid directly from the forces acting between constituent molecules through a statistical mechanical approach. Latter developments, like non-local DFT (NLDF)<sup>(3)</sup>, which makes an account for short range molecule correlation and therefore for the changes in the density profile around the pore walls, and quenched solid state DFT (QSDFT)<sup>(27)</sup>, which allows for heterogeneity of pore walls to be incorporated in the model, have improved the accuracy of the method.

The density functional theory approach can therefore simulate adsorption isotherms on pores of different geometries and sizes. By defining a pore geometry and running the simulation with a range of pore radii, a collection of isotherms is obtained. If an experimental isotherm is thought of as a sum of adsorption isotherms in different size pores, then it stands to reason that the preponderence of those pores can be calculated through deconvolution.

Since the DFT method can model adsorbate condensation behaviour, as well as micropore filling and multilayer adsorption, it can be used for multiscale pore size distribution. The downside is that DFT kernels are temperature, probe, pore-geometry and adsorbent specific and as such are not universally applicable.

#### 1.3.3. Predicting multicomponent adsorption

Until now, we have only referred to isotherms pertaining to the adsorption of a single adsorbate. However, besides gas storage, most if not all industrial applications of adsorbents involve multiple chemical species undergoing competitive adsorption. Experiments involving several adsorbents are generally difficult and time consuming. There is therefore a need to predict such multicomponent systems in order to rapidly screen for potentially interesting separations starting from pure component data.

To this end, the several methods have been devised, with perhaps the most common approach as considering the adsorbed phase as an analogue to a fluid mixture, in a manner analogous to the vacancy solution theory presented in subsection 1.2.9. This method, also known as ideal adsorbed solution theory (IAST) will be presented here. Other multicomponent theories such as real adsorbed solution theory (RAST) or the

## 1. Building a framework for adsorption data processing

Nitta model exist, but usually require more information such as specific surface binary activity coefficients, and are therefore less suited to a general approach. Furthermore, the IAST method has been proven<sup>(28,29)</sup> to be successful in the prediction of multicomponent adsorption even when considering adsorption in microporous materials such as MOFs.

Originally derived by Myers and Prausnitz, the IAST model<sup>(30)</sup> is based on three main assumptions. First, that the same surface area is available for all components. Then it is assumed that the mixture behaves like an ideal solution at constant spreading pressure and temperature. This means the spreading pressure of each component is the same as the surface potential of the mixture  $\pi$  and therefore the mean strength of interaction is equal between all molecules of solution. Finally the surface adsorbed phase is assumed to be in equilibrium with the gas phase. Equation 1.51 can then be written, where  $p_{i,g}$  is the partial pressure of the component in the gas phase,  $p_i^0(\pi)$  the pressure of that component which will give the same spreading pressure on the surface and  $x_i$  is its fraction in the adsorbed phase.

$$p_{i,g} = p_i^0(\pi)x_i \quad (1.51)$$

$$\frac{\pi A}{R_g T} = \int_0^{P_i^0} n_{ads,i} d \ln(p_i) \quad (1.52)$$

$$\sum_{i=1}^N x_i = 1 \quad (1.53)$$

For better consistency, fugacity can be used instead of pressure, in order to account for non-ideality of the gas phase, with a suitable equation of state required to relate them to bulk pressure. The pressure and spreading pressure are then related through the integrated Gibbs isotherm (Equation 1.52). As the sum of all fractions in the adsorbed phase is equal to unity (Equation 1.53), the equations can be solved for a given pressure and gas composition to give the fractions of each component in the adsorbed phase at the hypothetical pressure  $P_i^0$ . The total amount adsorbed can then be calculated.

$$\frac{1}{n_{ads,t}} = \sum_{i=1}^N \frac{x_i}{n_{ads,i}^0} \quad (1.54)$$

Finally, the number of moles adsorbed for each component is given by multiplying the total amount adsorbed by the fraction of each component.

$$n_{ads,i} = x_i n_{ads,t} \quad (1.55)$$

In order to calculate the spreading pressure, an adsorption model such as the ones presented in section 1.2 is required. By substituting the amount adsorbed ( $n_{ads}$ ) in Equation 1.51 and calculation of the resulting integral, an expression for spreading pressure can be determined. The integral can only be evaluated analytically in the case of a few

models, for example in the previously mentioned Henry, Langmuir and multi-site Langmuir, BET, Quadratic and Temkin models. In other cases, a numerical approach must be used for its calculation. An alternative to using a model is to use an interpolation method between recorded experimental points to approximate the amount adsorbed at a pressure  $p$ . Numerical quadrature is then used to evaluate the integral and obtain the spreading pressure.

## 1.4. pyGAPS overview

After a description of adsorption and its application to porous material characterisation and prediction of mixture adsorption, the code which was developed to tackle this type of processing can be presented.

The software was imagined for use in two types of scenario. First, as a command line interface, in common data science environments such as IPython and Jupyter. The typical user working in these environments is likely to be processing a small batch of results at a time, and is interested in obtaining the results in graphical form. For this type of application, the framework should provide an unobtrusive way of importing the user data, as well as present an API which does not require extensive knowledge of processing methods. Finally, a graphing environment is required which will allow the user to visualise their dataset and results.

The second envisaged application is related to bulk data processing. Requirements here shift towards parameter control, scripting and extensibility. The framework API should offer the option to change implicit parameters, select calculation limits and return the results in a numerical form for further processing. This type of application is also likely to require storage of isotherms in a database or under other types of data files.

### 1.4.1. Core structure

In order to offer a clear structuring of functionality, pyGAPS introduces several classes which abstract data and concepts for facile interaction (Figure 1.2). The classes are intuitively named: `Isotherm`, `Sample` and `Adsorbent`.

#### The Isotherm class

The `Isotherm` class is a representation of an adsorption isotherm i.e. a function of the amount adsorbed, or loading, with pressure at a fixed temperature. The class also contains other information relating to the isotherm, such as the material name and batch it describes, the adsorbate used and other user-defined properties.

This relationship can be defined in two ways:

- individual pressure-loading pairs of points which have been recorded as part of a measurement or
- as a mathematical function describing the relationship between the two properties.

## 1. Building a framework for adsorption data processing

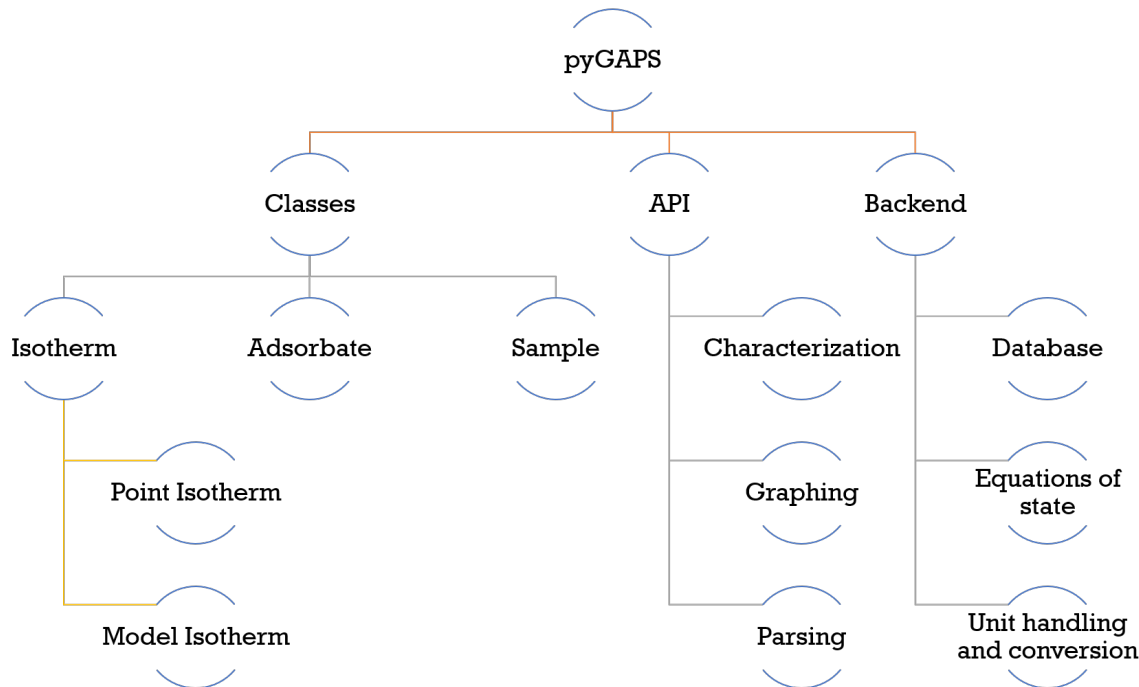


**Figure 1.2.:** An overview of the package structure

As such, the `Isotherm` class is used as a parent class for two subclasses: the `PointIsotherm` which contains datapoints and the `ModelIsotherm`, containing a model such as Henry, Langmuir etc. The two classes are interchangeable as they share most methods and properties. Once an instance of an `Isotherm` class is created, it can then be used for the processing, conversion and graphing capabilities of `pyGAPS`.

### The Sample class

The isotherm classes contain the name and batch of the sample they are measured on in a string format. The user might want to specify other information about the material, such as the date of synthesis or the material's density, as well as store this information in the database. For this case, `pyGAPS` provides the `Sample` class. The framework uses the string values in the isotherm to connect an `Isotherm` instance to a specific `Sample`. If sample-related properties are needed for processing, such as conversion of an isotherm from a mass basis to a volume basis, this class will be checked for the required data.

### The Adsorbate class

Finally, in order for many of the calculations included in `pyGAPS` to be performed, properties of the adsorbate used are needed e.g. liquid density, vapour pressure etc. The `Adsorbate` class is provided for this purpose, which is connected to an `Isotherm` class in an identical manner as the `Sample` class. The physical properties are calculated automatically through an equation of state, either the open source CoolProp library<sup>(31)</sup> or

## 1. Building a framework for adsorption data processing

the NIST-made REFPROP<sup>(32)</sup>, if available on the user's computer. The properties can also be retrieved from the internal database or specified by the user.

### 1.4.2. Creation of an Isotherm

An Isotherm can be created either from the command line directly or through an import from a supported format. For direct creation, the code takes two kinds of inputs: the data itself, in the form of a `pandas.DataFrame`, and the isotherm parameters describing it. Only four parameters are strictly required: the material name, the material batch, the adsorbate used and the experimental temperature. Other parameters can be passed as well and will be stored in the isotherm class. An example code can be seen in Listing 1.1.

The `DataFrame` must contain a column containing the pressure points and one containing the corresponding loading points of the isotherm. Other columns can also be passed, when secondary data such as enthalpy of adsorption is present at each measurement point. These columns will be saved in the case of the `PointIsotherm` class and can be plotted afterwards. The framework can automatically attempt to determine the adsorption and desorption branches, by analysing the input data. Alternatively, the user can manually specify which points belong to each branch.

If no unit data is specified in the constructor, the framework will assume that the isotherm is in units of  $\text{mmol g}^{-1}$  loading as a function of bar. Both the units and the basis can be specified, as it is explained in a latter section.

Finally, the data is saved in the newly created class or used to generate parameters for a model such as BET, Langmuir, etc., in the case of a `PointIsotherm` and `ModelIsotherm` respectively. The creation of `Sample` and `Adsorbate` instances is similar.

Alternatively, the isotherm can be imported from a file containing a format that is recognised by pyGAPS. Parsing from suitably structured JSON, CSV and Excel files is supported.

Both `PointIsotherms` and `ModelIsotherm` can be created from an instance of the other, by using the available functions. As an example, a model is automatically generated from the previous isotherm using the function in Listing 1.2, which fits all available models and selects the one with the lowest residuals between the fitted function and the real data.

**Listing 1.2:** Guessing the best model

```
1 model = pygaps.ModelIsotherm.from_pointisotherm(iso, guess_model=True)

Attempting to model using Henry
Model Henry success, rmse is 7.42
Attempting to model using Jensen-Seaton
Modelling using Jensen-Seaton failed
.....
Best model fit is Quadratic
```

## 1. Building a framework for adsorption data processing

**Listing 1.1:** Creating the PointIsotherm

```
1 point_isotherm = pygaps.PointIsotherm(
2
3     # First the pandas.DataFrame with the points
4     # and the keys to what the columns represent.
5
6     pandas.DataFrame({
7         'pressure' : [1, 2, 3, 4, 5, 3, 2],
8         'loading' : [1, 2, 3, 4, 5, 3, 2],
9         'enthalpy' : [15, 15, 15, 15, 15, 15, 15],
10        'xrd_peak_1' : [0, 0, 1, 2, 2, 1, 0],
11    }),
12
13    loading_key='loading',                      # The loading column
14    pressure_key='pressure',                    # The pressure column
15    other_keys=['enthalpy',                   ,
16                'xrd_peak_1'],                 # The columns containing other data
17
18    # Some of the unit parameters can be
19    # specified if desired.
20
21    pressure_mode='absolute',                  # absolute pressure
22    pressure_unit='bar',                      # with units of bar
23    adsorbent_basis='mass',                   # adsorbent mass basis
24    adsorbent_unit='kg',                      # with units of kg
25    loading_basis='mass',                     # loading mass basis
26    loading_unit='g',                        # with units of g
27
28    # Finally the isotherm description
29    # parameters are passed.
30
31    'sample_name' : 'carbon',                 # Required
32    'sample_batch' : 'X1',                    # Required
33    'adsorbate' : 'nitrogen',                # Required
34    't_exp' : 77,                           # Required
35    't_act' : 150,                          # Recognised / named
36    'user' : 'Username',                    # Recognised / named
37    'DOI' : '10.000/mydoi',                 # Unknown / user specific
38 )
```

### 1.4.3. Units

When computers work with physical data, units are often a matter that introduces confusion. Here we explain how `pyGAPS` handles units and other physical world concepts such as relative pressure and mass or volume basis.

The following dimensions can be specified for an Isotherm: the measurement *pressure*, the quantity of guest adsorbed or *loading* and the amount of adsorbent material the loading is reported on, or *adsorbent*.

Pressure can be reported either in an absolute value, in several common units such as bar, torr, Pa, or as *relative pressure*, absolute pressure divided by the saturation vapour pressure of the adsorbate at the respective measurement temperature. Conversions between the two modes are automatic and handled internally.

Both the *loading* and *adsorbent* can be reported in three different bases: a molar basis, a mass basis or a volume basis. Within each basis different units are recognised and can be easily converted. The conversions between bases can also easily performed if the required conversion factors (i.e. molar mass and density) are available. For *loading*, these factors are automatically calculated internally using the available equation of state, while for the *adsorbent* they should be provided by the user in the respective `Sample` class.

### 1.4.4. Workflow

Once an isotherm object is created, it will be used for all further processing. The class contains methods which can be used to inspect the data visually, or retrieve parts of the isotherm such as the adsorption or desorption branches with user-chosen limits or units. Singular values of pressure or loading can be calculated, either through interpolation in the case of a `PointIsotherm` or by evaluation of the internal model in the `ModelIsotherm`. For an isotherm with datapoints, these can also be converted into different units or modes.

Characterisation functions take an isotherm object as their first parameter. This is the case for the BET area, Langmuir area, t-plot,  $\alpha_s$  plot, and pore size distribution methods. These characterisation functions attempt to automate as much of the process as possible. For example, the BET area limits are automatically calculated using the Rouquerol<sup>(18)</sup> method, with all the checks implemented into the code. In another example the straight line sections of the t-plot are determined automatically through a calculation of the second derivative of the transformed isotherm. For detailed control, there are available options for each individual method, such as manual BET limits, different thickness functions for the t-plot or Kelvin-based mesoporous pore distribution methods, custom parameters for the Horvath-Kawazoe microporous pore distribution, custom DFT or NLDFT kernels and more. The results are returned in a numerical form for further processing, or can be directly displayed if the `verbose` parameter is passed.

### 1.4.5. Characterisation using pyGAPS

#### BET and Langmuir surface area

pyGAPS comes with several common methods used to determine surface area, some with theoretical basis like the IUPAC-recommended BET method and some empirical, such as the t-plot method.

Starting from an isotherm object, it is easy to calculate the nitrogen BET area of a sample of UiO-66(Zr) MOF by using the code in Listing 1.3. The framework automatically applies the methodology described in section 1.3.1 to find the optimum pressure range. The `verbose=True` option prints a short text with all the calculation variables as well as graphing the BET and Rouquerol plots (Figure 1.3). The user can override automatic pressure range selection by using the range parameter (`limits=(0.05, 0.3)`).

**Listing 1.3:** Calculating a BET area

```
1 area_dict = pygaps.area_BET(isotherm, verbose=True)
```

```
BET surface area: a = 1277 m2/g
Minimum pressure point chosen is 0.005 and maximum is 0.034
The slope of the BET fit:      s = 76.344
The intercept of the BET fit: i = 0.052
BET constant:                C = 1463
Amount for a monolayer:       n = 0.01309 mol/g
```

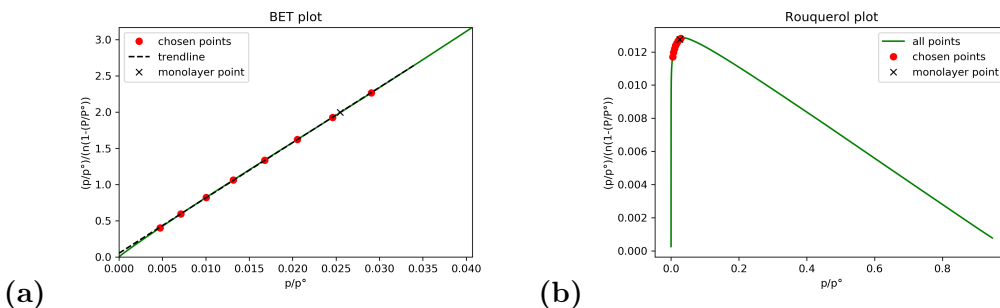


**Figure 1.3.:** Output from the BET area function (a) the BET plot showing the selected points for fitting the equation, as well as the location of the statistical monolayer and (b) the Rouquerol plot for this calculation.

Similarly to the BET area, the Langmuir area is calculated by using the code in Listing 1.4. The framework will alert the user if the correlation is not linear in the selected range. In this example, the surface area of a nitrogen isotherm measured on a MCM-41 sample is calculated. Here the `verbose=True` option prints a short text with all the calculation results, as well as generating the Langmuir plot as seen in Figure 1.4a. If desired the user can override automatic pressure range selection as seen in the second example in Listing 1.4.

**Listing 1.4:** Calculating a Langmuir area

```
1 area_dict = pygaps.area_langmuir(isotherm, verbose=True)
```

## 1. Building a framework for adsorption data processing

| WARINING The correlation is not linear!

```
1 area_dict = pygaps.area_langmuir(isotherm,
2                                     limits=(0.05, 0.3),
3                                     verbose=True)
```

```
Langmuir surface area: a = 415 m2/g
Minimum pressure point chosen is 0.0 and maximum is 0.194
The slope of the Langmuir line: s = 234.968
The intercept of the Langmuir line: i = 1.607
The Langmuir constant is: K = 146
Amount for a monolayer: n = 0.00426 mol/g
```

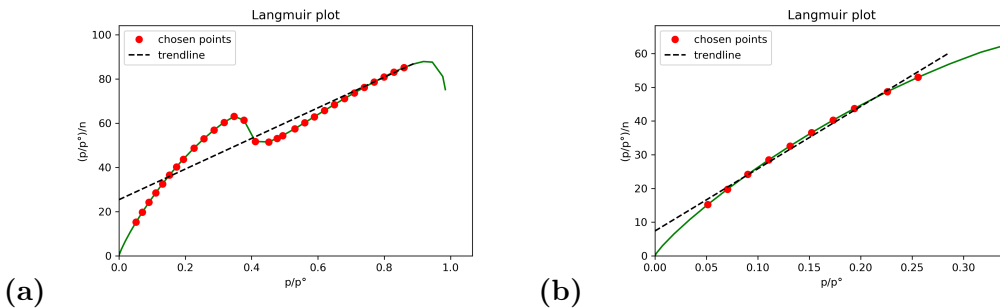


**Figure 1.4.:** Output from the Langmuir area function (a) the Langmuir plot showing the automatic fitting attempt which generates a warning and (b) a manually selected pressure range for the Langmuir plot.

### The t-plot Method and $\alpha_s$ Method

The t-plot method requires a model for the thickness of the adsorbed layer, as described in section 1.3.1. The two equations presented there have been implemented in pyGAPS. These t-curves are selected by name as parameters in the functions that use them. The user can also define their own t-curve as a function and pass it as a parameter.

When the t-plot function is called without any parameters except an isotherm, the framework will attempt to find plateaus in the data and automatically fit them with a straight line, returning a dictionary with the slope, intercept, calculated pore volume and specific area for each linear region found. The same MCM-41 nitrogen isotherm analysed in the previous section is used in Listing 1.5. The first command will generate the graph in Figure 1.5a.

The first linear region in Figure 1.5a can be attributed to adsorption on the mesopore surface, while the second one represents adsorption on the available surface after mesopore filling. Therefore, the surface area values calculated for the first and second region correspond to the area of the mesopores and the external particle area, respectively. As only one pore filling event occurs, the pore volume calculated for the second region gives us the mesopore volume. We can obtain a more accurate result for the surface area

## 1. Building a framework for adsorption data processing

**Listing 1.5:** Generating a t-plot

```

1 # using automatic region detection
2 pygaps.t_plot(isotherm, verbose=True)
3
4 # specifying a manual region
5 pygaps.t_plot(isotherm, limits=(0.3,0.44), verbose=True)
6
7 # using the Halsey thickness curve
8 pygaps.t_plot(isotherm, thickness_model='Halsey', verbose=True)
9
10 # defining a custom t-curve to use in the t-plot
11 def carbon_model(relative_p):
12     return 0.88*(relative_p**2) + 6.45*relative_p + 2.98
13
14 pygaps.t_plot(isotherm, thickness_model=carbon_model, verbose=True)

```

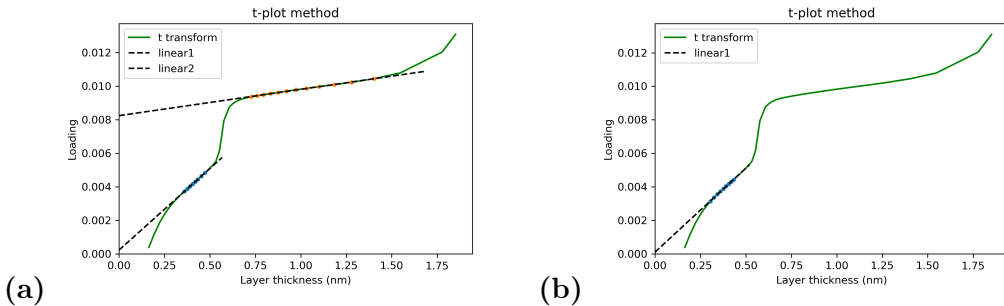


**Figure 1.5.:** Output from the t-plot method function (a) an automatically obtained t-plot with the calculated fit regions and (b) a manually selected range for the t-plot.

by fitting the first linear region to a zero intercept through manual region selection, as shown in the second example in Listing 1.5.

Finally, the framework allows for the thickness model to be substituted with an user-provided function which will be used for the t-plot. Usage of a carbon black-type thickness curve is presented in the last example in Listing 1.5.

To generate an  $\alpha_s$ -plot in pyGAPS, both an analysis isotherm and a reference isotherm must be supplied as shown in Listing 1.6, using the same isotherm as for the t-plot. In this example, the reference isotherm is measured on non-porous silica. The reference material area can be specified by using the `reference_area` parameter. If not specified, it is automatically calculated by applying the BET method to the reference isotherm.

**Listing 1.6:** Generating an  $\alpha_s$ -plot

```

1 pygaps.alpha_s(isotherm,
2                 reference_isotherm=isotherm_r,
3                 verbose=True)

```

## 1. Building a framework for adsorption data processing

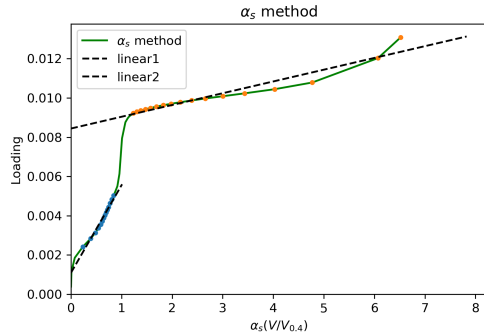


**Figure 1.6.:** Output from the  $\alpha_s$ -plot function showing two automatically fit regions.

### Pore size distribution calculations

Both mesoporous, microporous and DFT fitting routines can be used to calculate a pore size distribution in pyGAPS. While the generation of DFT kernels is outside the scope of the framework, it is able to use user-provided kernels to fit adsorption isotherms, and comes with a basic kernel applicable for N<sub>2</sub> adsorption at 77 K on carbon slit pores.

The MCM-41 sample is a mesoporous material, which is expected to have a well-defined pore size in the range of 2.5 nm to 5 nm. The BJH method can be readily applied on the desorption branch of the measured isotherm, through the code in Listing 1.7. The Harkins and Jura thickness function is automatically selected, while the default cylindrical pore geometry is used.

**Listing 1.7:** PSD using the BJH method

```

1 result_dict = pygaps.mesopore_size_distribution(
2     charact_iso,
3     psd_model='BJH',
4     verbose=True
5 )

```

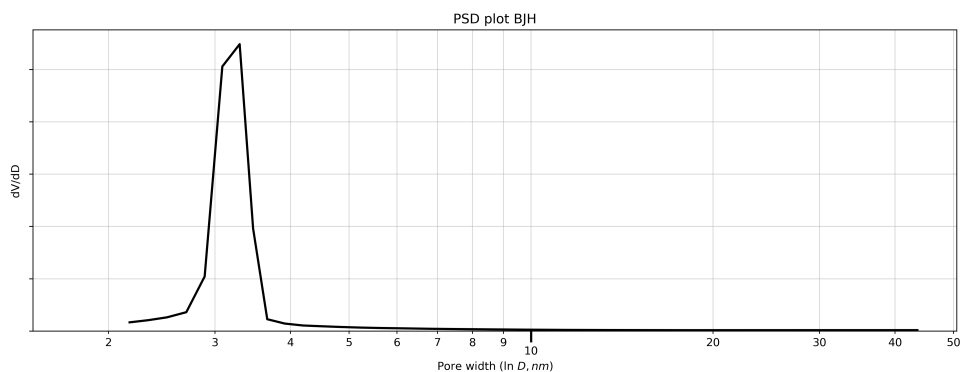


**Figure 1.7.:** BJH pore size distribution

The resulting pore size distribution in Figure 1.7, confirms the analysis, with a single

## 1. Building a framework for adsorption data processing

sharp pore distribution at 3 nm.

A microporous analysis cannot be performed on MCM-41, since it does not contain any pores under 2.5 nm, where such methods are applicable. Instead, the UiO-66(Zr) isotherm is used. This MOF has two micropores, a tetrahedral and octahedral one which are accessible through an 8 Å window. The HK method is used for calculating the pore size distribution, as displayed in Listing 1.8.

**Listing 1.8:** Using the HK method for PSD

```
1 # Calling the HK micropore method with the
2 # Saito-Foley oxide surface parameters
3 result_dict = pygaps.micropore_size_distribution(
4     isotherm,
5     psd_model='HK',
6     adsorbent_model='OxideIon(SF)',
7     verbose=True
8 )
9 # Defining a custom adsorbate parameter dictionary
10 # and using it in the HK method
11 adsorbate_params = {
12     'magnetic_susceptibility': 3.6e-35,
13     'molecular_diameter': 0.3,
14     'polarizability': 1.76e-30,
15     'surface_density': 6.71e+18
16 }
17 result_dict = pygaps.micropore_size_distribution(
18     isotherm,
19     psd_model='HK',
20     adsorbent_model='OxideIon(SF)',
21     adsorbate_model=adsorbate_params,
22     verbose=True
23 )
```

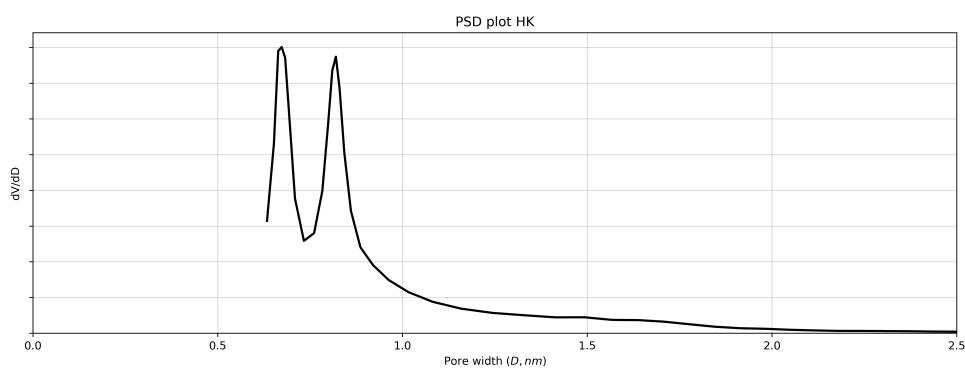


**Figure 1.8.:** Pore size distribution calculated through the Horvath-Kawazoe method on the UIO-66(Zr) sample

## 1. Building a framework for adsorption data processing

The pyGAPS framework contains the required physical properties for the most commonly used adsorbates in its database, as well as properties from literature for several materials: the original parameters developed by Horvath and Kawazoe for a carbon surface<sup>(26)</sup> and the oxide surface parameters published by Saito and Foley.<sup>(33)</sup> The user can also provide a custom dictionary for these parameters when calling the function as can be seen in the second example in Listing 1.8.

Finally, to determine a pore size distribution using DFT kernel fitting, the `dft_size_distribution` function is used. The function takes an `Isotherm` object and a path to a CSV representation of the DFT kernel. The code then loads the kernel either from disk or memory and applies a minimization function on the sum of squared differences of the sum of all individual kernel isotherms to generate the contribution of each as per the following equation:

$$f(x) = \sum_{p=p_0}^{p=p_x} \left( n_{p,\text{exp}} - \sum_{w=w_0}^{w=w_y} n_{p,\text{kernel}} X_w \right)^2 \quad (1.56)$$

The user can specify their own kernel in a CSV format or, alternatively, use the internal kernel included with the framework. This kernel is only applicable on N<sub>2</sub> adsorption at 77K on carbon slit-like pores in the range of 0.4 nm to 10 nm.

The isotherm measured on the microporous carbon Takeda 5A is used as an input for the DFT fitting routine (Listing 1.9), using the available internal kernel. The resulting PSD shows that the material is not completely microporous, with a wide mesopore component present.

**Listing 1.9:** DFT size distribution in pyGAPS

```
1 result_dict = pygaps.dft_size_distribution(
2     charact_iso,
3     'internal',
4     verbose=True
5 )
```

better  
graph

## Multicomponent adsorption modelling

The pyGAPS framework includes a modified version of the pyIAST code<sup>(34)</sup> which has been adapted to work with the `Isotherm` classes. Both model isotherms and real data can be used for IAST, with spreading pressure being calculated through the underlying isotherm model or through interpolation, respectively as detailed in subsection 1.3.3.

As an example, two common case studies will be examined: the capture of CO<sub>2</sub> from N<sub>2</sub> and separation of propane and propylene. Models of isotherms recorded on a Takeda 5A microporous carbon are generated using the automatic fitting functionality. The original isotherms and the best-fitting models are displayed in Figure 1.10a for the CO<sub>2</sub>-N<sub>2</sub> pair and in Figure 1.11a for the C<sub>3</sub>H<sub>8</sub>-C<sub>3</sub>H<sub>6</sub> pair.

## 1. Building a framework for adsorption data processing

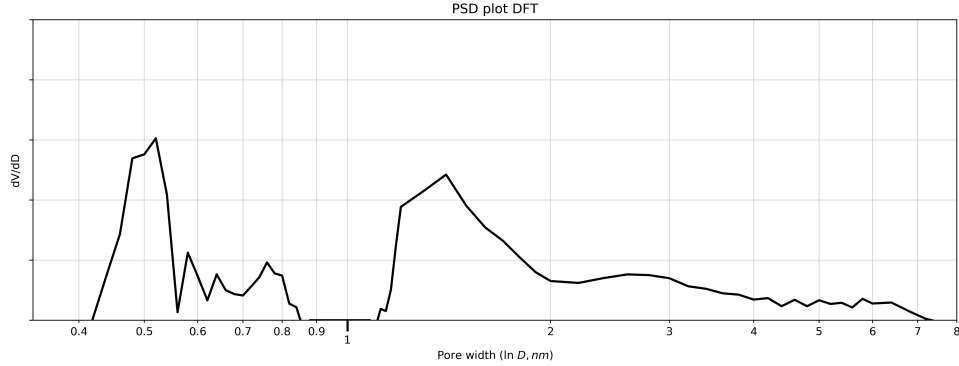


**Figure 1.9.:** Pore size distribution calculated through the DFT fitting on the Takeda 5A carbon

For the carbon dioxide separation, all equilibrium points for the adsorbed and gaseous phases are simulated at different proportions of the two gases, with a total pressure of 1 bar. To do this we use the `pygaps.iast_vle()` function which produces an analogue of a vapour-liquid equilibrium at a specified pressure for a binary mixture. The resulting graph can be seen in Figure 1.11b. As expected, the predicted adsorbed mixture is rich in carbon dioxide. Selectivity can also be calculated in a single point, with the value at a concentration analogous to flue gas of 15% CO<sub>2</sub> being 16.5.

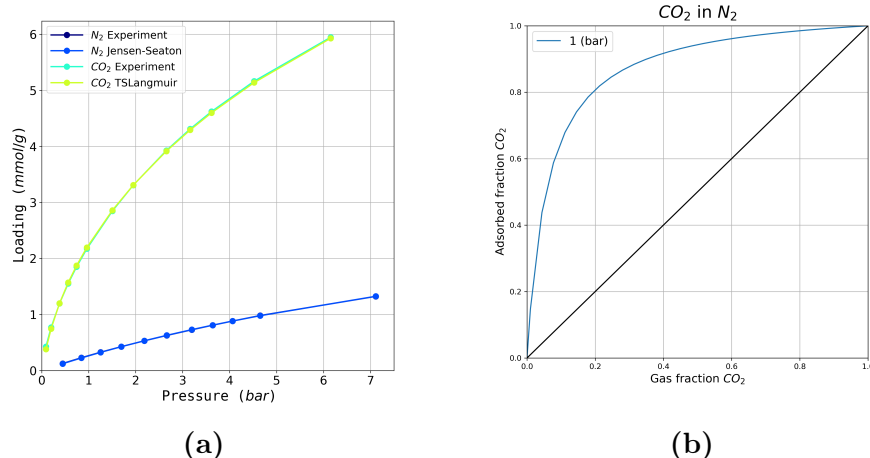


**Figure 1.10.:** Modelling binary adsorption of CO<sub>2</sub> and N<sub>2</sub>: (a) the pure component isotherms and their best fit models and (b) the predicted composition of the gaseous and adsorbed phase for different fractions of CO<sub>2</sub> at 1 bar

For the propane-propylene separation, the selectivity for propane in an equimolar mixture of the two gases is simulated within a pressure range of 0.1 bar to 5 bar. It can be seen that there is little or no preference for the unsaturated molecule, though the selectivity increases slightly at pressures above 1 bar.

## 1. Building a framework for adsorption data processing

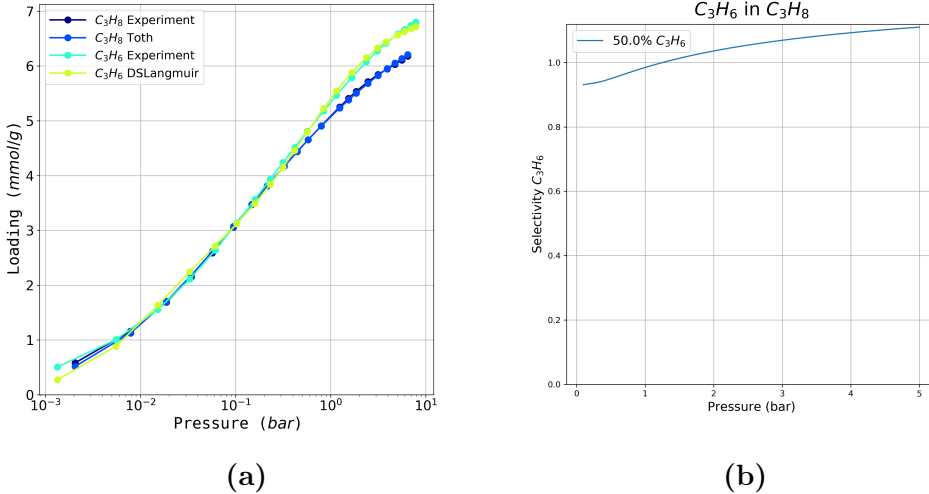


**Figure 1.11.:** Modelling binary adsorption of a propane-propylene mixture: (a) the pure-component isotherms and their best fit models and (b) the predicted selectivity of propane adsorption of a 50–50% mixture in a range of pressure from 0.1 to 7 bar

## 1.5. Processing a large adsorption dataset

With the capability for fast processing afforded by pyGAPS, we now turn to using it on an available database of adsorption isotherms. The goal is to test the speed and accuracy of the calculations, as well as to obtain a description of the dataset. Further insights may be obtained from benchmarking of different KPIs, or assessing the reliability of the available data.

### 1.5.1. The NIST ISODB dataset

The NIST/ARPA-E database of adsorbent materials (ISODB) is a comprehensive set of adsorption isotherms which have been systematically collected from peer-reviewed literature. The data includes measurements on a wide range of materials, from carbon, zeolite, and silica to MOFs and other such PCPs. This resource is a useful tool for reference purposes, as it contains isotherms with many probes at various temperatures. Furthermore, due to the availability of an application programming interface (API), isotherm data can be easily accessed. As such, this database is a great source of data for the kind of large-scale processing which pyGAPS is designed for.

The entire dataset in the NIST adsorption database was downloaded using the publicly available API. This yielded  $\approx 26000$  isotherms. In order to narrow down the dataset and ensure comparability the following sorting was performed.

- Only isotherms measured with an adsorbate that is available in the pyGAPS database were selected, to allow for calculations using the internal equation of state.

## 1. Building a framework for adsorption data processing

- Isotherms which could not be converted to  $\text{mmol g}^{-1}$  were discarded outright. This includes data reported on a volume basis of material (as the material density is unknown), simulation data which is reported in units such as molecules per unit cage and fractional coverage isotherms. All remaining isotherms were then converted into  $\text{mmol g}^{-1}$  using the pyGAPS conversion functionality to ensure a consistent unit set.
- No isotherms with less than 6 measurement points were considered, as it was considered to be the bare minimum required for characterisation.
- Possible outliers were removed from the data by selecting only isotherms recorded under 100 bar, with maximum capacities under 100 mmol and with a temperature of under 443 K. Any such isotherms are likely errors in the data collection process and have little to no physical meaning.

The process of data collation reduced the number of isotherms to  $\approx 15800$ . A distribution of the isotherms as a function of adsorbate and temperature can be found in Figure 1.12a. We can see that most isotherms are recorded at either 77 K, 273 K or 298 K as these temperatures are readily available through immersion in liquid nitrogen, water-ice mixture, or a thermally controlled water bath respectively. In total, isotherms measured with all 20 probe gasses available in pyGAPS are found in the database, including four common vapours and all linear saturated hydrocarbons up to a carbon number of four.

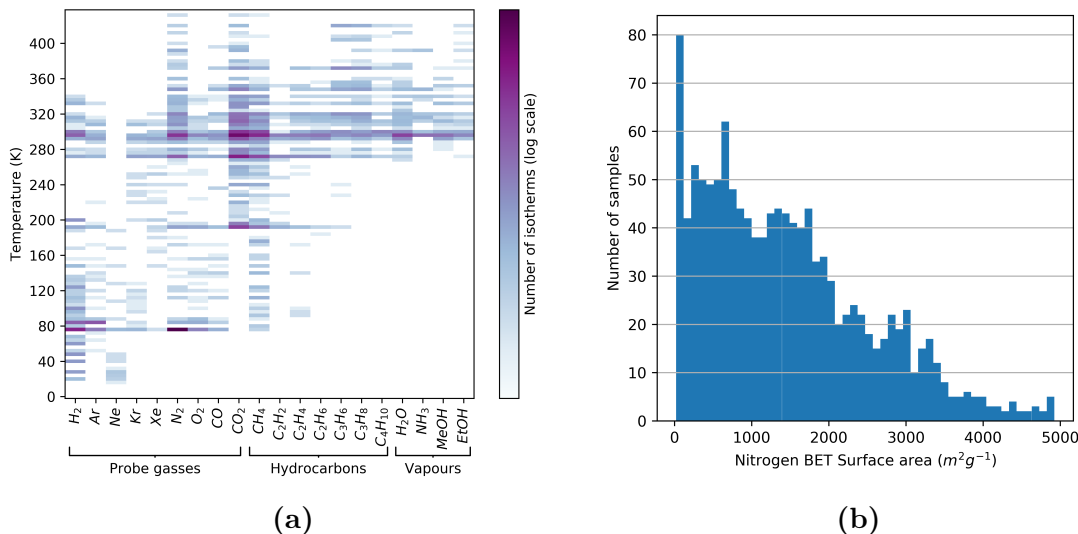


**Figure 1.12.:** A graphical description of the NIST ISODB dataset. (a) The selected 15800 isotherms presented per adsorbate used and temperature at which the measurement took place. (b) Calculated BET surface area with nitrogen at 77 K for all available isotherms.

## 1. Building a framework for adsorption data processing

For an initial round of data processing with pyGAPS, only isotherms recorded with nitrogen at 77K were selected. These make up  $\approx 3500$  datapoints, recorded on more than 2200 materials. The BET surface area was then computed for each isotherm, with a distribution as seen in Figure 1.12b. Unfortunately, as many isotherms do not have enough points in the low pressure region, computing a well-defined BET surface area is impossible. In total, only around a third of the isotherms had enough data for this purpose. Several materials are seen to be essentially non-porous with around 80 isotherms recorded having a BET area of less than  $100 \text{ m}^2/\text{g}$ . As expected, a decrease in number of samples is seen with increasing surface area reflecting the lower preponderence of highly porous materials due to the challenges involved in their creation. Overall, while this initial calculation does not impart any further insights, it serves as an useful overview of the ISODB dataset.

### 1.5.2. A comparison between surface area calculation methods

The Langmuir surface area is an often-reported alternative to the, now standard, BET method area. With such a large dataset at our disposal, we can take the opportunity to observe the differences between results obtained with the two methods. If the Langmuir area is calculated with implicit parameters, by taking the entire available isotherm for the fitting routine, the correlation between the two methods looks like Figure 1.13a. The two results do not agree well, with the Langmuir surface area usually higher than the BET value for the same isotherm. This is a consequence of the Langmuir model assuming adsorption up to a single monolayer with other characteristic phenomena such as multilayer adsorption, pore condensation or multiple types of adsorption types unable to be accounted for.

If the partial pressure range is narrowed, by only using points up to  $0.15 p/p_0$ , the correlation improves dramatically, with near-overlap when the area is below  $2000 \text{ m}^2/\text{g}$ . In this case the selection corresponds to a region below the “knee” of an ideal BET isotherm, before the statistical monolayer is filled.

In truth, the choice of either model is strictly applicable to determine the accessible area of microporous materials, due to adsorption in such samples being dominated by pore filling mechanisms rather than monolayer formation. However, as detailed by Rouquerol et al.<sup>(35)</sup> and then also shown through comparing simulated and experimental data by Walton and Snurr<sup>(36)</sup>, the results produced by judicious application of such models can relate well to the actual surface areas of MOFs.

### 1.5.3. Variability of the dataset

Before a deeper dive into attempting to relate adsorption isotherm derived parameters to structural properties, an analysis of the reliability of the data from the NIST ISODB should be performed.

The material with the most recorded isotherms is CuBTC, with 122 datapoints. A spread of the calculated BET surface areas, together with the “ideal” area of this MOF as obtained through simulations<sup>(37)</sup> is presented in Figure 1.14. To verify if the variability

## 1. Building a framework for adsorption data processing

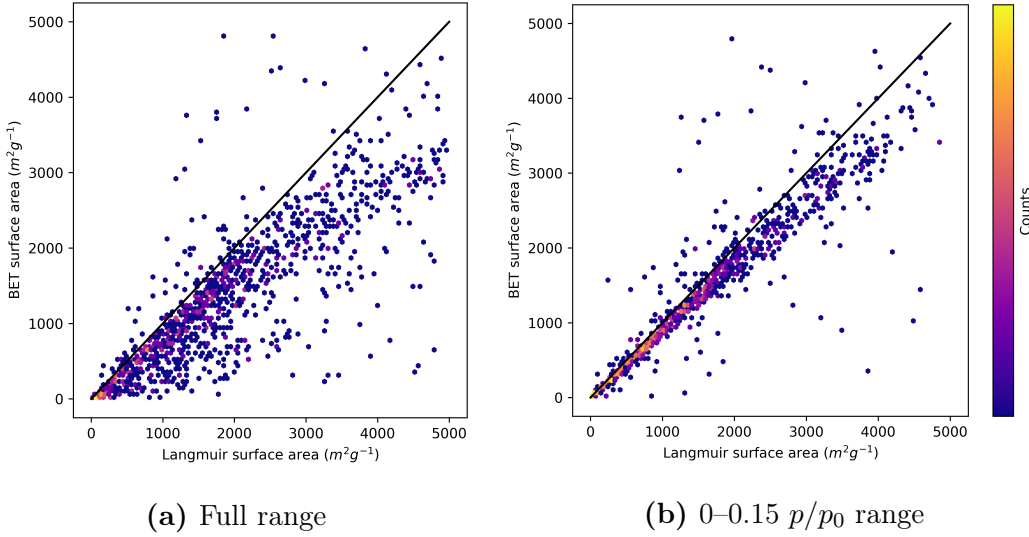


**Figure 1.13.:** Correlation between Langmuir-calculated and BET-calculated surface areas. The black line is a guide for the eye at  $S_{Lang} = S_{BET}$ .

is due to uncertainty in the surface area calculation a secondary metric, namely the capacity at 0.5  $p/p_0$  has been calculated and its distribution plotted alongside that of the BET area. The identical trends in both parameters show that there is an inherent uncertainty in the dataset. The results not only have a large standard deviation, but also do not have a typical normal distribution one would expect from repeated sampling of a physical property.

Instead, three normal distributions appear to emerge, one with a median around  $500 \text{ m}^2/\text{g}$ , a second around  $1300 \text{ m}^2/\text{g}$  and a third with a median around  $1900 \text{ m}^2/\text{g}$  which also corresponds to the nitrogen accessible surface area determined through simulation. As the NIST data also records the DOI for each isotherm, each measurement can be traced to the publication it originated in. By cherry-picking several studies from each normal distribution we can find that the low surface areas correspond to data measured on modified versions of CuBTC, such as shaped samples ( $640 \text{ m}^2/\text{g}$ )<sup>(38)</sup>, hollow nanoparticles ( $450 \text{ m}^2/\text{g}$ )<sup>(39)</sup> or nanoplates ( $803 \text{ m}^2/\text{g}$ ).<sup>(40)</sup> Studies selected from materials with higher surface area showed no consistent underlying cause for the

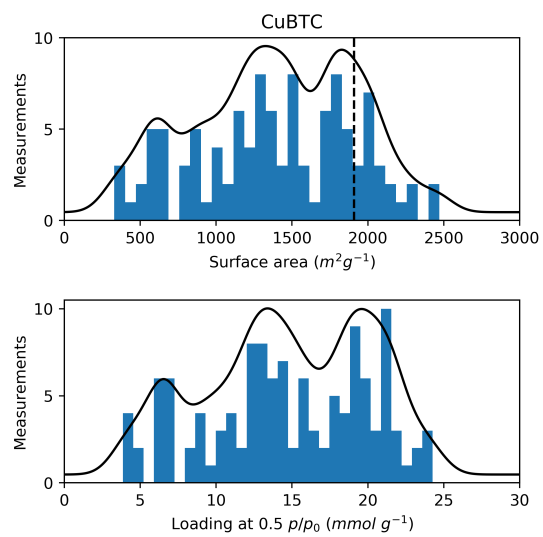


**Figure 1.14.:** A histogram and estimate of the probability density function for (top) BET surface area and (bottom) loading at half saturation pressure for CuBTC. The black dotted line is the simulated surface area of this MOF.

## 1. Building a framework for adsorption data processing

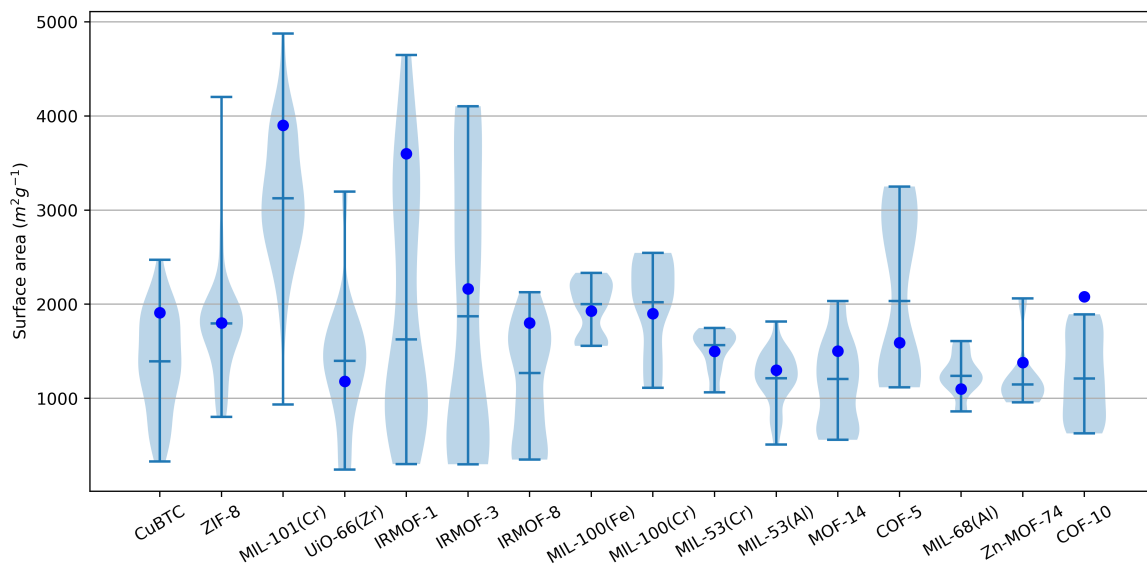


**Figure 1.15.:** A violin plot of the calculated surface areas for all available nitrogen isotherms on the top 16 MOFs. The top and bottom lines in each plot are the limits for the surface area values. The shaded area is a kernel-density estimate of the probability density function using Gaussian kernels. The median of each dataset is displayed as the horizontal line between the two limits. Finally, the round blue point is the BET surface area of the material as reported in literature through simulation or optimised synthesis.

variability, although some can be accounted for through synthesis method such as mechanochemical synthesis ( $1700\text{ m}^2/\text{g}$ )<sup>(41)</sup>, or structural defects ( $2050\text{ m}^2/\text{g}$ ).<sup>(42)</sup>

To extend the analysis to other materials, MOFs with at least 8 recorded nitrogen isotherms were selected, resulting in 16 materials. A violin plot with the results of the calculation for these datapoints is presented in Figure 1.15. The blue points mark the surface area of the material as obtained from literature or simulated values or, if not available, the original synthesis paper of the MOF in question. It is obvious that, in most cases, there is a large spread in the calculated values, with some samples such as IRMOF-1, IRMOF-3 and MIL-101(Cr) having a surface area anywhere between  $200\text{ m}^2/\text{g}$  to  $5000\text{ m}^2/\text{g}$ . Other materials, such as ZIF-8, the MIL-53 family and MIL-100(Fe) have less variability in their surface areas, although can still be shifted by  $200$  to  $500\text{ m}^2/\text{g}$ .

Similar concerns have been raised for  $\text{H}_2$ <sup>(43)</sup> and  $\text{CO}_2$ <sup>(44)</sup> measurements. Recently, Sholl and co-workers<sup>(37)</sup> have published a report putting into question the reproducibility of adsorption isotherms, using  $\text{CO}_2$  adsorption data from the NIST adsorption database. Their findings highlight a large variability inherent to reported isotherms as on average “one in five  $\text{CO}_2$  isotherms [...] cannot be used to provide information that is qualitatively reliable about the properties of the material”. However, in their paper they do not

## 1. Building a framework for adsorption data processing

explore the reasons behind the origin of such large variations.

The underlying cause for the poor reproducibility of adsorption isotherms, particularly those measured on metal organic frameworks, is not easy to pinpoint. A large contribution to this divergence is likely accounted for through the variation introduced by the sample preparation method and adsorption apparatus. For example, a recent NIST interlaboratory study in which CO<sub>2</sub> isotherms were recorded on a reference material<sup>(45)</sup>, received six out of thirteen initial datasets outside the uncertainty range. Errors were determined to arise from sample mass measurement, insufficient activation conditions or improper choice of an equation of state. Other method-specific sources of error exist, such as the lack of a buoyancy correction when using a gravimetric system or a void volume correction when using a volumetric system, both of which can be made if an accurate determination of sample skeletal density is performed. Finally, small differences in thermal gradients, pressure transducer readings, and even the altitude at which the measurement takes place (if a phase change bath is used to control temperature) can also impact the final isotherm.

Such variation is likely minimised when using state-of-the-art adsorption equipment, which eliminates many of the concerns associated with adsorption methodology. *In situ* activation, internal consistency checks for pressure transducers, automatic measurement of skeletal density and associated corrections, reference cells for saturation pressure determination and many other sanity checks are implemented in these machines.

However, it is often the case that the most important factor in the repeatability MOF and porous material adsorption isotherms is not the measurement procedure, but rather the material itself. As evidenced by the closer look at the CuBTC dataset, synthesis method, crystallinity, material form, particle size and contribution of defects all have an impact on the resulting adsorption behaviour of the material. As such,

## 1.6. Conclusion

In this chapter, a framework for adsorption data processing is presented, which focuses on standardisation of porous material characterisation through adsorption methods and large-scale processing of isotherms. Prediction of multicomponent adsorption is also made possible through IAST calculations.

Analysis of isotherms available in the NIST ISODB, which are collated from literature, shows a comprehensive set of data. A brief comparison between two ways of calculating surface area (BET and Langmuir) as applied to nitrogen isotherms confirms long-standing recommendations of their applicability and use. However, further analysis reveals a large variability present in the measured isotherms on metal-organic frameworks.

The other chapters in this thesis will explore the origin of some of this variability, such as inherent defects in the material (chapter 3), changes introduced by shaping (chapter 4) and of course, through unique behaviours of MOFs such as flexibility arising from its building blocks (chapter 5).

## BIBLIOGRAPHY

### Bibliography

- [1] Elliott P. Barrett, Leslie G. Joyner, and Paul P. Halenda. The Determination of Pore Volume and Area Distributions in Porous Substances. I. Computations from Nitrogen Isotherms. *Journal of the American Chemical Society*, 73(1):373–380, January 1951. ISSN 0002-7863. doi: 10.1021/ja01145a126.
- [2] N.A. Seaton, J.P.R.B. Walton, and N. Quirke. A new analysis method for the determination of the pore size distribution of porous carbons from nitrogen adsorption measurements. *Carbon*, 27(6):853–861, 1989. ISSN 00086223. doi: 10.1016/0008-6223(89)90035-3.
- [3] P. Tarazona, U. Marini Bettolo Marconi, and R. Evans. Phase equilibria of fluid interfaces and confined fluids: Non-local versus local density functionals. *Molecular Physics*, 60(3):573–595, February 1987. ISSN 0026-8976, 1362-3028. doi: 10.1080/00268978700100381.
- [4] Dan Siderius, Vincent Shen, and Russell Johnson. NIST / ARPA-E Database of Novel and Emerging Adsorbent Materials, NIST Standard Reference Database 205, 2015.
- [5] Salil U. Rege and Ralph T. Yang. A simple parameter for selecting an adsorbent for gas separation by pressure swing adsorption. *Separation science and technology*, 36(15):3355–3365, 2001.
- [6] M.W. Ackley, A.B. Stewart, G.W. Henzler, F.W. Leavitt, F. Notaro, and M.S. Kane. PSA apparatus and process using adsorbent mixtures, February 2000. US Patent 6,027,548.
- [7] Andrew D. Wiersum, Jong-San Chang, Christian Serre, and Philip L. Llewellyn. An Adsorbent Performance Indicator as a First Step Evaluation of Novel Sorbents for Gas Separations: Application to Metal–Organic Frameworks. *Langmuir*, 29(10):3301–3309, March 2013. ISSN 0743-7463, 1520-5827. doi: 10.1021/la3044329.
- [8] Irving Langmuir. The Adsorption of Gases on Plane Surfaces of Glass, Mica and Platinum. *Journal of the American Chemical Society*, 40(9):1361–1403, September 1918. ISSN 0002-7863, 1520-5126. doi: 10.1021/ja02242a004.
- [9] Stephen Brunauer, P. H. Emmett, and Edward Teller. Adsorption of Gases in Multimolecular Layers. *Journal of the American Chemical Society*, 60(2):309–319, February 1938. ISSN 0002-7863, 1520-5126. doi: 10.1021/ja01269a023.
- [10] Mikhail Temkin. Kinetics of ammonia synthesis on promoted iron catalyst. *Acta Phys. Chim. USSR*, 12:327–356, 1940.
- [11] Cory M. Simon, Jihan Kim, Li-Chiang Lin, Richard L. Martin, Maciej Haranczyk, and Berend Smit. Optimizing nanoporous materials for gas storage. *Physical*

## BIBLIOGRAPHY

- Chemistry Chemical Physics*, 16(12):5499, 2014. ISSN 1463-9076, 1463-9084. doi: 10.1039/c3cp55039g.
- [12] C. R. C. Jensen and N. A. Seaton. An isotherm equation for adsorption to high pressures in microporous adsorbents. *Langmuir*, 12(11):2866–2867, 1996.
  - [13] Terrell L. Hill. *An Introduction to Statistical Thermodynamics*. Dover Publications, New York, 1986. ISBN 978-0-486-65242-9.
  - [14] Alan L. Myers. Thermodynamics of adsorption in porous materials. *AICHE Journal*, 48(1):145–160, January 2002. ISSN 00011541. doi: 10.1002/aic.690480115.
  - [15] Solot Suwanayuen and Ronald P. Danner. A gas adsorption isotherm equation based on vacancy solution theory. *AICHE Journal*, 26(1):68–76, January 1980. ISSN 00011541. doi: 10.1002/aic.690260112.
  - [16] T. W. Cochran, R. L. Kabel, and R. P. Danner. Vacancy solution theory of adsorption using Flory-Huggins activity coefficient equations. *AICHE Journal*, 31(2): 268–277, February 1985. ISSN 0001-1541, 1547-5905. doi: 10.1002/aic.690310214.
  - [17] Matthias Thommes, Katsumi Kaneko, Alexander V. Neimark, James P. Olivier, Francisco Rodriguez-Reinoso, Jean Rouquerol, and Kenneth S W Sing. Physisorption of gases, with special reference to the evaluation of surface area and pore size distribution (IUPAC Technical Report). *Pure and Applied Chemistry*, 87(9-10): 1051–1069, 2015. ISSN 13653075. doi: 10.1515/pac-2014-1117.
  - [18] Jean Rouquerol, Françoise Rouquerol, Philip L. Llewellyn, Guillaume Maurin, and Kenneth Sing. *Adsorption by Powders and Porous Solids : Principles, Methodology and Applications*. 2013. ISBN 978-0-08-097035-6.
  - [19] George Halsey. Physical Adsorption on Non-Uniform Surfaces. *The Journal of Chemical Physics*, 16(10):931–937, October 1948. ISSN 0021-9606, 1089-7690. doi: 10.1063/1.1746689.
  - [20] William D. Harkins and George Jura. Surfaces of Solids. XIII. A Vapor Adsorption Method for the Determination of the Area of a Solid without the Assumption of a Molecular Area, and the Areas Occupied by Nitrogen and Other Molecules on the Surface of a Solid. *Journal of the American Chemical Society*, 66(8):1366–1373, August 1944. ISSN 0002-7863, 1520-5126. doi: 10.1021/ja01236a048.
  - [21] B Lippens. Studies on pore systems in catalysts V. The t method. *Journal of Catalysis*, 4(3):319–323, June 1965. ISSN 00219517. doi: 10.1016/0021-9517(65)90307-6.
  - [22] D. Atkinson, A.I. McLeod, and K. S. W. Sing. Adsorptive properties of microporous carbons: Primary and secondary micropore filling. *Journal de Chimie Physique*, 81: 791–794, 1984. ISSN 0021-7689. doi: 10.1051/jcp/1984810791.

## BIBLIOGRAPHY

- [23] Jean Rouquerol, Gino V. Baron, Renaud Denoyel, Herbert Giesche, Johan Groen, Peter Klobes, Pierre Levitz, Alexander V. Neimark, Sean Rigby, Romas Skudas, Kenneth Sing, Matthias Thommes, and Klaus Unger. The characterization of macroporous solids: An overview of the methodology. *Microporous and Mesoporous Materials*, 154:2–6, May 2012. ISSN 13871811. doi: 10.1016/j.micromeso.2011.09.031.
- [24] Duong D Do. *Adsorption Analysis: Equilibria and Kinetics: (With CD Containing Computer Matlab Programs)*, volume 2 of *Series on Chemical Engineering*. Imperial College Press, September 1998. ISBN 978-1-86094-130-6 978-1-78326-224-3. doi: 10.1142/p111.
- [25] D. Dollimore and G.R R. Heal. Pore-size distribution in typical adsorbent systems. *Journal of Colloid and Interface Science*, 33(4):508–519, August 1970. ISSN 00219797. doi: 10.1016/0021-9797(70)90002-0.
- [26] Geza Horvath and Kunitaro Kawazoe. Method for the calculation of effective pore size distribution in molecular sieve carbon. *Journal of Chemical Engineering of Japan*, 16(6):470–475, 1983. ISSN 1881-1299. doi: 10.1252/jcej.16.470.
- [27] Alexander V. Neimark, Yangzheng Lin, Peter I. Ravikovitch, and Matthias Thommes. Quenched solid density functional theory and pore size analysis of micro-mesoporous carbons. *Carbon*, 47(7):1617–1628, June 2009. ISSN 00086223. doi: 10.1016/j.carbon.2009.01.050.
- [28] Naomi F. Cessford, Nigel A. Seaton, and Tina Düren. Evaluation of Ideal Adsorbed Solution Theory as a Tool for the Design of Metal–Organic Framework Materials. *Industrial & Engineering Chemistry Research*, 51(13):4911–4921, April 2012. ISSN 0888-5885, 1520-5045. doi: 10.1021/ie202219w.
- [29] Timothy Van Heest, Stephanie L. Teich-McGoldrick, Jeffery A. Greathouse, Mark D. Allendorf, and David S. Sholl. Identification of Metal–Organic Framework Materials for Adsorption Separation of Rare Gases: Applicability of Ideal Adsorbed Solution Theory (IAST) and Effects of Inaccessible Framework Regions. *The Journal of Physical Chemistry C*, 116(24):13183–13195, June 2012. ISSN 1932-7447, 1932-7455. doi: 10.1021/jp302808j.
- [30] A. L. Myers and J. M. Prausnitz. Thermodynamics of mixed-gas adsorption. *AIChE Journal*, 11(1):121–127, January 1965. ISSN 0001-1541, 1547-5905. doi: 10.1002/aic.690110125.
- [31] Ian H. Bell, Jorrit Wronski, Sylvain Quoilin, and Vincent Lemort. Pure and Pseudo-pure Fluid Thermophysical Property Evaluation and the Open-Source Thermophysical Property Library CoolProp. *Industrial & Engineering Chemistry Research*, 53 (6):2498–2508, February 2014. ISSN 0888-5885, 1520-5045. doi: 10.1021/ie4033999.

## BIBLIOGRAPHY

- [32] Eric Lemmon. NIST Reference Fluid Thermodynamic and Transport Properties Database: Version 9.0, NIST Standard Reference Database 23, 1989.
- [33] A. Saito and H. C. Foley. Curvature and parametric sensitivity in models for adsorption in micropores. *AICHE Journal*, 37(3):429–436, March 1991. ISSN 0001-1541. doi: 10.1002/aic.690370312.
- [34] Cory M. Simon, Berend Smit, and Maciej Haranczyk. PyIAST: Ideal adsorbed solution theory (IAST) Python package. *Computer Physics Communications*, 200: 364–380, 2016. ISSN 00104655. doi: 10.1016/j.cpc.2015.11.016.
- [35] J. Rouquerol, P. Llewellyn, and F. Rouquerol. Is the bet equation applicable to microporous adsorbents? In *Studies in Surface Science and Catalysis*, volume 160, pages 49–56. Elsevier, 2007. ISBN 978-0-444-52022-7. doi: 10.1016/S0167-2991(07)80008-5.
- [36] Krista S. Walton and Randall Q. Snurr. Applicability of the BET Method for Determining Surface Areas of Microporous Metal-Organic Frameworks. *Journal of the American Chemical Society*, 129(27):8552–8556, July 2007. ISSN 0002-7863, 1520-5126. doi: 10.1021/ja071174k.
- [37] Jongwoo Park, Joshua D. Howe, and David S. Sholl. How Reproducible Are Isotherm Measurements in Metal-Organic Frameworks? *Chemistry of Materials*, 29(24):10487–10495, December 2017. ISSN 0897-4756, 1520-5002. doi: 10.1021/acs.chemmater.7b04287.
- [38] Junmin Li, Jiangfeng Yang, Libo Li, and Jinping Li. Separation of CO<sub>2</sub>/CH<sub>4</sub> and CH<sub>4</sub>/N<sub>2</sub> mixtures using MOF-5 and Cu<sub>3</sub>(BTC)<sub>2</sub>. *Journal of Energy Chemistry*, 23 (4):453–460, July 2014. ISSN 20954956. doi: 10.1016/S2095-4956(14)60171-6.
- [39] Ai-Ling Li, Fei Ke, Ling-Guang Qiu, Xia Jiang, Yi-Min Wang, and Xing-You Tian. Controllable synthesis of metal-organic framework hollow nanospheres by a versatile step-by-step assembly strategy. *CrystEngComm*, 15(18):3554, 2013. ISSN 1466-8033. doi: 10.1039/c2ce26636a.
- [40] Li Peng, Jianling Zhang, Jianshen Li, Buxing Han, Zhimin Xue, and Guanying Yang. Surfactant-directed assembly of mesoporous metal-organic framework nanoplates in ionic liquids. *Chemical Communications*, 48(69):8688, 2012. ISSN 1359-7345, 1364-548X. doi: 10.1039/c2cc34416e.
- [41] Maria Klimakow, Peter Klobes, Andreas F. Thünemann, Klaus Rademann, and Franziska Emmerling. Mechanochemical Synthesis of Metal-Organic Frameworks: A Fast and Facile Approach toward Quantitative Yields and High Specific Surface Areas. *Chemistry of Materials*, 22(18):5216–5221, September 2010. ISSN 0897-4756, 1520-5002. doi: 10.1021/cm1012119.

## BIBLIOGRAPHY

- [42] Gokhan Barin, Vaiva Krungleviciute, Oleksii Gutov, Joseph T. Hupp, Taner Yildirim, and Omar K. Farha. Defect Creation by Linker Fragmentation in Metal–Organic Frameworks and Its Effects on Gas Uptake Properties. *Inorganic Chemistry*, 53(13):6914–6919, July 2014. ISSN 0020-1669, 1520-510X. doi: 10.1021/ic500722n.
- [43] D. P. Broom and M. Hirscher. Irreproducibility in hydrogen storage material research. *Energy & Environmental Science*, 9(11):3368–3380, 2016. ISSN 1754-5692, 1754-5706. doi: 10.1039/C6EE01435F.
- [44] Laura Espinal, Dianne L. Poster, Winnie Wong-Ng, Andrew J. Allen, and Martin L. Green. Measurement, Standards, and Data Needs for CO<sub>2</sub> Capture Materials: A Critical Review. *Environmental Science & Technology*, 47(21):11960–11975, November 2013. ISSN 0013-936X, 1520-5851. doi: 10.1021/es402622q.
- [45] H. G. T. Nguyen, L. Espinal, R. D. van Zee, M. Thommes, B. Toman, M. S. L. Hudson, E. Mangano, S. Brandani, D. P. Broom, M. J. Benham, K. Cychosz, P. Bertier, F. Yang, B. M. Krooss, R. L. Siegelman, M. Hakuman, K. Nakai, A. D. Ebner, L. Erden, J. A. Ritter, A. Moran, O. Talu, Y. Huang, K. S. Walton, P. Billemont, and G. De Weireld. A reference high-pressure CO<sub>2</sub> adsorption isotherm for ammonium ZSM-5 zeolite: Results of an interlaboratory study. *Adsorption*, July 2018. ISSN 0929-5607, 1572-8757. doi: 10.1007/s10450-018-9958-x.

# A. Common characterisation techniques

pictures?

## A.1. Thermogravimetry

Thermogravimetry (TGA) is a standard laboratory technique where the weight of a sample is monitored while ambient temperature is controlled. Changes in sample mass can be correlated to physical events, such as adsorption, desorption, sample decomposition or oxidation, depending on temperature and its rate of change.

TGA experiments are carried out on approximately 15 mg of sample with a TA Instruments Q500 up to 800 °C. The sample is placed on a platinum crucible and sealed in a temperature controlled oven, under gas flow of  $40 \text{ cm}^3 \text{ min}^{-1}$ . Experiments can use a blanket of either air or argon. The temperature ramp can be specified directly and should be chosen to ensure that the sample is in equilibrium with the oven temperature and no thermal conductivity effects come into play. Alternatively, a dynamic “Hi-Res” mode can be used which allows for automatic cessation of heating rate while the sample undergoes mass loss.

The main purpose of thermogravimetry as used in this thesis is the determination of sample decomposition temperature, to ensure that thermal activation prior to adsorption is complete and that all guest molecules have been removed without loss of structure. To this end, experiments are performed under an inert atmosphere (argon), and the sample activation temperature is chosen as 50 °C to 100 °C lower than the sample decomposition temperature.

## A.2. Bulk density determination

Bulk density is a useful metric for the industrial use of adsorbent materials, as their volume plays a critical role in equipment sizing.

Bulk density is determined by weighing 1.5 ml empty glass vessels and settling the MOFs inside. Powder materials are then added in small increments and settled through vibration between each addition. The full vessel is finally weighed, which allowed the bulk density to be determined. The same cell is used in all experiments, with cleaning through sonication between each experiment.

## A. Common characterisation techniques

### A.3. Skeletal density determination

True density or skeletal density is determined through gas pycnometry in a Microtrac-BEL BELSORP-max apparatus. Helium is chosen as the fluid of choice as it is assumed to be non-adsorbing.

The volume of a glass sample cell ( $V_c$ ) is precisely measured through dosing of the reference volume with helium up to ( $p_1$ ), then opening the valve connecting the two and allowing the gas to expand up to ( $p_2$ ). Afterwards approximately 50 mg of sample are weighed and inserted in a glass sample cell. After sample activation using the supplied electric heater to ensure no solvent residue is left in the pores, the same procedure is repeated to determine the volume of the cell and the adsorbent. With the volume of the sample determined, the density can be calculated by.

$$V_s = V_c + \frac{V_r}{1 - \frac{p_1}{p_2}} \quad (\text{A.1})$$

### A.4. Nitrogen physisorption at 77 K

Nitrogen adsorption experiments are carried out on a Micromeritics Triflex apparatus. Approximately 60 mg of sample are used for each measurement. Empty glass cells are weighed and filled with the samples, which are then activated in a Micromeritics Smart VacPrep up to their respective activation temperature under vacuum and then back-filled with an inert atmosphere. After sample activation, the cells are re-weighed to determine the precise sample mass. The cells are covered with a porous mantle which allows for a constant temperature gradient during measurement by wicking liquid nitrogen around the cell. Finally, the cells are immersed in a liquid nitrogen bath and the adsorption isotherm is recorded using the volumetric method. A separate cell is used to condense the adsorptive throughout the measurement for accurate determination of its saturation pressure.

### A.5. Vapour physisorption at 298 K

Vapour adsorption isotherms throughout this work are measured using a MicrotracBEL BELSORP-max apparatus in vapour mode. Glass cells are first weighed and then filled with about 50 mg of sample. The vials are then heated under vacuum up to the activation temperature of the material and re-weighed in order to measure the exact sample mass without adsorbed guests. The cells are then immersed in a mineral oil bath kept at 298 K. To ensure that the cold point of the system occurs in the material and to prevent condensation on cell walls, the reference volume, dead space and vapour source are temperature controlled through an insulated enclosure.

## BIBLIOGRAPHY

### A.6. Gravimetric isotherms

The gravimetric isotherms in this thesis are obtained using a commercial Rubotherm GmbH balance. Approximately 1 g of dried sample is used for these experiments. Samples are activated *in situ* by heating under vacuum. The gas is introduced using a step-by-step method, and equilibrium is assumed to have been reached when the variation of weight remained below 30 µg over a 15 min interval. The volume of the sample is determined from a blank experiment with helium as the non-adsorbing gas and used in combination with the gas density measured by the Rubotherm balance to compensate for buoyancy.

### A.7. High throughput isotherm measurement

A high-throughput gas adsorption apparatus is presented for the evaluation of adsorbents of interest in gas storage and separation applications. This instrument is capable of measuring complete adsorption isotherms up to 50 bar on six samples in parallel using as little as 60 mg of material. Multiple adsorption cycles can be carried out and four gases can be used sequentially, giving as many as 24 adsorption isotherms in 24 h.<sup>(1)</sup>

### A.8. Powder X-ray diffraction

### A.9. Nuclear magnetic resonance

## Bibliography

- [1] Andrew D. Wiersum, Christophe Giovannangeli, Dominique Vincent, Emily Bloch, Helge Reinsch, Norbert Stock, Ji Sun Lee, Jong-San Chang, and Philip L. Llewellyn. Experimental Screening of Porous Materials for High Pressure Gas Adsorption and Evaluation in Gas Separations: Application to MOFs (MIL-100 and CAU-10). *ACS Combinatorial Science*, 15(2):111–119, February 2013. ISSN 2156-8952. doi: 10.1021/co300128w.

## B. Synthesis method of referenced materials

### B.1. Takeda 5A reference carbon

The Takeda 5A carbon was purchased directly from the Takeda corporation. The sample was activated at 250 °C under secondary vacuum (5 mbar) before any measurements.

full characterization

### B.2. MCM-41 controlled pore glass

MCM-41 (Mobil Composition of Matter No. 41) is a mesoporous silica ( $\text{SiO}_2$ ) material with a narrow pore distribution. First synthesised by the Mobil Oil Corporation, it is produced through templated synthesis using mycelle-forming surfactants. The material referenced in this thesis was purchased from Sigma-Aldrich. The activation procedure consists of heating at 250 °C under secondary vacuum (5 mbar).

### B.3. Zr fumarate MOF

The synthesis of the Zr fumarate was performed in Peter Behren's group in Hannover, through modulated synthesis. This MOF can only be synthesised through the addition of a modulator, in this case fumaric acid, to the ongoing reactor, as detailed in the original publication.<sup>(1)</sup>

The procedure goes as follows:  $\text{ZrCl}_4$  (0.517 mmol, 1 eq) and fumaric acid (1.550 mmol, 3 eq) are dissolved in 20 mL N,N-dimethylformamide (DMF) and placed in a 100 mL glass flask at room temperature. 20 equivalents of formic acid were added. The glass flasks were Teflon-capped and heated in an oven at 120 °C for 24 h. After cooling, the white precipitate was washed with 10 mL DMF and 10 mL ethanol, respectively. The washing process was carried out by centrifugation and redispersion of the white powder, which was then dried at room temperature over night

### B.4. UiO-66(Zr) for defect study

The UiO-66(Zr) sample preparation was adapted from Shearer et al. <sup>(2)</sup> as follows:  $\text{ZrCl}_4$  (1.55 g, 6.65 mmol), an excess of terephthalic acid (BDC) (1.68 g, 10.11 mmol), HCl 37 % solution (0.2 mL, 3.25 mmol) and N,N'-dimethylformamide (DMF) (200 mL,

## B. Synthesis method of referenced materials

2.58 mol) were added to a 250 mL pressure resistant Schott bottle. The mixture was stirred for 10 min, followed by incubation in a convection oven at 130 °C for 24 h. The resulting white precipitate was washed with fresh DMF (3× 50 mL) followed by ethanol (3× 50 mL) over the course of 48 h and dried at 60 °C. After drying, the sample was activated on a vacuum oven by heating at 200 °C under vacuum for 12 h. The yield was 78 % white microcrystalline powder. Before the experiment, the sample was calcined at 200 °C under vacuum (5 mbar) to remove any residual solvents from the framework.

### B.5. UiO-66(Zr) for shaping study

The scaled-up synthesis of UiO-66(Zr) was carried out in a 5 L glass reactor (Reactor Master, Syrris, equipped with a reflux condenser and a Teflon-lined mechanical stirrer) according to a previously reported method.<sup>(3)</sup> In short, 462 g (2.8 mol) of H<sub>2</sub>BDC (98%) was initially dissolved in 2.5 L of dimethyl formamide (DMF, 2.36 kg, 32.3 mol) at room temperature. Then, 896 g (2.8 mol) of ZrOCl<sub>2</sub> · 8H<sub>2</sub>O (98%) and 465 mL of 37% HCl (548 g, 15 mol) were added to the mixture. The molar ratio of the final ZrOCl<sub>2</sub> · 8H<sub>2</sub>O/H<sub>2</sub>BDC/DMF/HCl mixture was 1 : 1 : 11.6 : 5.4. The reaction mixture was vigorously stirred to obtain a homogeneous gel. The mixture was then heated to 423 K at a rate of 1 K min<sup>-1</sup> and maintained at this temperature for 6 h in the reactor without stirring, leading to a crystalline UiO-66(Zr) solid. The resulting product (510 g) was recovered from the slurry by filtration, redispersed in 7 L of DMF at 333 K for 6 h under stirring, and recovered by filtration. The same procedure was repeated twice, using methanol (MeOH) instead of DMF. The solid product was finally dried at 373 K overnight.

### B.6. MIL-100(Fe) for shaping study

The synthesis of the MOF for the shaping study was done at the KRICT institute using a previously published method.<sup>(4)</sup> To synthesise the MIL-100(Fe) material Fe(NO<sub>3</sub>)<sub>3</sub> was completely dissolved in water. Then, trimesic acid (BTC) was added to the solution; the resulting mixture was stirred at room temperature for 1h. The final composition was Fe(NO<sub>3</sub>)<sub>3</sub> · 9 H<sub>2</sub>O:0.67 BTC:*n* H<sub>2</sub>O (*x*= 55–280). The reactant mixture was heated at 433 K for 12 h using a Teflon-lined pressure vessel. The synthesized solid was filtered and washed with deionized (DI) water. Further washing was carried out with DI water and ethanol at 343 K for 3 h and purified with a 38 mM NH<sub>4</sub>F solution at 343 K for 3 h. The solid was finally dried overnight at less than 373 K in air.

### B.7. MIL-127(Fe) for shaping study

MIL-127(Fe) was synthesized by reaction of Fe(ClO<sub>4</sub>)<sub>3</sub> · 6 H<sub>2</sub>O (3.27 g, 9.2 mmol) and C<sub>16</sub>N<sub>2</sub>O<sub>8</sub>H<sub>6</sub> (3.3 g) in DMF (415 mL) and hydrofluoric acid (5 M, 2.7 mL) at 423 K in a Teflon flask. The obtained orange crystals were placed in DMF (100 mL) and

## BIBLIOGRAPHY

stirred at ambient temperature for 5 h. The final product was kept at 375 K overnight. MIL-127(Fe) was synthesized by reaction of  $\text{Fe}(\text{ClO}_4)_3 \cdot 6\text{H}_2\text{O}$  (3.27 g, 9.2 mmol) and  $\text{C}_{16}\text{N}_2\text{O}_8\text{H}_6$  (3.3 g) in DMF (415 mL) and hydrofluoric acid (5 M, 2.7 mL) at 423 K in a Teflon flask. The obtained orange crystals were placed in DMF (100 mL) and stirred at ambient temperature for 5 h. The final product was kept at 375 K overnight.

## Bibliography

- [1] Gesa Wißmann, Andreas Schaate, Sebastian Lilienthal, Imke Bremer, Andreas M. Schneider, and Peter Behrens. Modulated synthesis of Zr-fumarate MOF. *Micro-porous and Mesoporous Materials*, 152:64–70, April 2012. ISSN 13871811. doi: 10.1016/j.micromeso.2011.12.010.
- [2] Greig C. Shearer, Sachin Chavan, Jayashree Ethiraj, Jenny G. Vitillo, Stian Svelle, Unni Olsbye, Carlo Lamberti, Silvia Bordiga, and Karl Petter Lillerud. Tuned to Perfection: Ironing Out the Defects in Metal–Organic Framework UiO-66. *Chemistry of Materials*, 26(14):4068–4071, July 2014. ISSN 0897-4756, 1520-5002. doi: 10.1021/cm501859p.
- [3] Florence Ragon, Patricia Horcajada, Hubert Chevreau, Young Kyu Hwang, U-Hwang Lee, Stuart R. Miller, Thomas Devic, Jong-San Chang, and Christian Serre. In Situ Energy-Dispersive X-ray Diffraction for the Synthesis Optimization and Scale-up of the Porous Zirconium Terephthalate UiO-66. *Inorganic Chemistry*, 53(5):2491–2500, March 2014. ISSN 0020-1669, 1520-510X. doi: 10.1021/ic402514n.
- [4] Felix Jeremias, Stefan K. Henninger, and Christoph Janiak. Ambient pressure synthesis of MIL-100(Fe) MOF from homogeneous solution using a redox pathway. *Dalton Transactions*, 45(20):8637–8644, 2016. ISSN 1477-9226, 1477-9234. doi: 10.1039/C6DT01179A.